Molecular Therapy
Oncolytics
Original Article

Galectin-3 inhibition boosts the therapeutic efficacy of Semliki Forest virus in pediatric osteosarcoma

Guillermo Herrador-Cañete,[1,2,3] Marta Zalacain,[1,2,4] Sara Labiano,[1,2,4] Virginia Laspidea,[1,2,4] Montserrat Puigdelloses,[1,2,4] Lucía Marrodan,[1,2,4] Marc Garcia-Moure,[1,2,4] Marisol Gonzalez-Huarriz,[1,2,4] Javier Marco-Sanz,[1,2,4] Iker Ausejo-Mauleon,[1,2,4] Daniel de la Nava,[1,2,4] Reyes Hernández-Osuna,[1,2,4] Javier Martínez-García,[1,3] Noelia Silva-Pilipich,[1,3] Elisabeth Gurucega,[1,5] Ana Patiño-García,[1,2,4] Rubén Hernández-Alcoceba,[1,3] Cristian Smerdou,[1,3] and Marta M. Alonso[1,2,4]

[1]Health Research Institute of Navarra (IdiSNA), Pamplona 31008, Spain; [2]Solid Tumor Program, Cima Universidad de Navarra, Pamplona 31008, Spain; [3]Gene Therapy and Regulation of Gene Expression Program, Cima Universidad de Navarra, Pamplona 31008, Spain; [4]Department of Pediatrics, Clínica Universidad de Navarra, Pamplona 31008, Spain; [5]Bioinformatics Platform, Cima Universidad de Navarra, Pamplona 31008, Spain

The outcomes of metastatic and nonresponder pediatric osteosarcoma patients are very poor and have not improved in the last 30 years. These tumors harbor a highly immunosuppressive environment, making existing immunotherapies ineffective. Here, we evaluated the use of Semliki Forest virus (SFV) vectors expressing galectin-3 (Gal3) inhibitors as therapeutic tools, since both the inhibition of Gal3, which is involved in immunosuppression and metastasis, and virotherapy based on SFV have been demonstrated to reduce tumor progression in different tumor models. *In vitro*, inhibitors based on the Gal3 amino-terminal domain alone (Gal3-N) or fused to a Gal3 peptide inhibitor (Gal3-N-C12) were able to block the binding of Gal3 to the surface of activated T cells. *In vivo*, SFV expressing Gal3-N-C12 induced strong antitumor responses in orthotopic K7M2 and MOS-J osteosarcoma tumors, leading to complete regressions in 47% and 30% of mice, respectively. Pulmonary metastases were also reduced in K7M2 tumor-bearing mice after treatment with SFV-Gal3-N-C12. Both the antitumor and antimetastatic responses were dependent on modulation of the immune system, primarily including an increase in tumor-infiltrating lymphocytes and a reduction in the immunosuppressive environment inside tumors. Our results demonstrated that SFV-Gal3-N-C12 could constitute a potential therapeutic agent for osteosarcoma patients expressing Gal3.

INTRODUCTION

Osteosarcoma is the most aggressive bone cancer in pediatric patients. It has an incidence of five cases per year per million in children ranging from 0 to 16 years old, which represents the first peak for this pathology.[1] A second peak appears in patients over 65 years old. Osteosarcoma originates from the aberrant production of osteoid and immature bone from mesenchymal stem cells.[2] Primary tumors may occur preferentially in the metaphyseal growth plates of the long bones, such as the femur (42% of cases), the tibia (19% of cases), and the humerus (10% of cases).[1] The first line of therapy for osteosarcoma consists of complete surgical resection of the primary tumor and metastases, combined with pre- and postsurgical chemotherapy (doxorubicin and cisplatin with or without subsequent treatment with high-dose methotrexate) for the most advanced stages.[3] However, although the 5-year survival rate is approximately 70% after localized tumor resection, for recurrent and metastatic patients this rate drops to less than 30%.[4] Current treatments have a very poor performance in these patients. Therefore, novel therapeutic strategies are urgently needed.

Therapeutic strategies based on virotherapy have been demonstrated to be a powerful tool for combating cancer, mainly solid tumors.[5] Viral vectors based on Semliki Forest virus (SFV), a self-replicating RNA virus, have been shown to be promising therapeutic agents for the treatment of different cancers.[6–10] Treatment of an aggressive orthotopic osteosarcoma mouse model with a propagation-competent SFV vector exhibited a potent oncolytic effect, induced a robust type I interferon (IFN) response, and produced an increase in survival among treated mice. However, treatment with this oncolytic SFV vector failed to generate long-term survivors.[11] These data indicate that although SFV vectors are potentially interesting, there is room to improve their efficacy. In this work, we hypothesized that arming SFV with an immunomodulatory agent could enhance its antitumor capacity. In this context, to improve the efficacy of an SFV vector in

Received 4 April 2022; accepted 7 July 2022;
https://doi.org/10.1016/j.omto.2022.07.004.

Correspondence: Cristian Smerdou, Health Research Institute of Navarra (IdiSNA), Pamplona 31008, Navarra, Spain.
E-mail: csmerdou@unav.es
Correspondence: Marta M Alons, Health Research Institute of Navarra (IdiSNA), Pamplona 31008, Navarra, Spain.
E-mail: mmalonso@unav.es

osteosarcoma tumors, non-propagation-competent SFV vectors were engineered to express inhibitors of galectin-3 (Gal3). Although these types of vectors cannot propagate owing to the lack of viral structural genes, they can replicate their RNA genomes, promoting a very high and transient expression of the transgene and inducing type I IFN responses and apoptosis in transduced cells.[12] The lack of propagation makes these vectors safer in comparison with fully propagative SFV virus.

Gal3 is a lectin protein upregulated in different types of tumors, such as osteosarcoma, in which its expression and secretion correlate with tumor progression and metastasis.[13–16] Apart from promoting the adhesion, migration, and invasion of osteosarcoma cells, this protein contributes to chemotherapy resistance.[17–19] Gal3 is also considered an immune checkpoint target in musculoskeletal tumor patients, including osteosarcoma patients.[20] In fact, tumor-secreted Gal3 promotes immunosuppression by triggering the polarization of macrophages/monocytes into protumoral M2 macrophages,[21] in which the binding of Gal3 to its binding protein (Gal3bp) induces the secretion of interleukin-6 (IL-6).[22] Gal3 can also capture cytokines such as IFN-γ and IL-12, reducing the CXCL9/10 gradient and thereby limiting the tumor infiltration of T cells.[23] Moreover, tumor-secreted Gal3 binds to glycosylated receptors on the surface of effector $CD4^+$ and $CD8^+$ T cells, promoting T cell receptor (TCR) exclusion, inactivation, and apoptosis, as well as reducing the expansion of plasmacytoid dendritic cells (pDCs).[24–26]

In this work, we demonstrated that local treatment of osteosarcoma tumors with SFV vectors expressing Gal3 inhibitors could promote a powerful specific antitumor immune response with the capacity to control not only local disease but also distant untreated lung metastases.

RESULTS

Galectin-3 and its binding protein are expressed in pediatric osteosarcoma patient and mouse model samples

To elucidate whether Gal-3 could be a therapeutic target in osteosarcoma, we first assessed its expression in patient biopsies (n = 6); the expression of Gal3bp, which is the main Gal3 ligand, and IL-6 was also evaluated. IL-6 promotes tumor progression and metastasis development and is upregulated following tumor-secreted Gal3bp binding to Gal3.[22,27] Pair-based analysis comparing healthy and primary tumor tissues from each patient showed a significant increase in the expression of Gal3bp ($p < 0.05$), whereas Gal3 ($p > 0.05$) and IL-6 ($p = 0.061$) expression was slightly augmented in tumor samples, but the difference did not reach significance (Figure 1A). Interestingly, we found a negative correlation between the expression of IL-6 and C1GALT1, an enzyme involved in the production of highly glycosylated ligands that reduces apoptosis triggered by the binding of Gal3 to tumor cells ($p < 0.01$; Figure 1A). Analysis of Gal3 and Gal3bp expression in human and murine osteosarcoma cell lines revealed that both molecules were highly expressed at the protein and mRNA levels (Figures 1B, 1C, and S1A). We also observed increased expression of Gal3 ($p > 0.05$), Gal3bp ($p < 0.01$), and IL-6 ($p > 0.05$) in primary tibia tumors from mice bearing orthotopic K7M2 osteosarcomas compared with normal tissue, similar to the results obtained with the patient samples (Figure 1D). This increase was more modest in pulmonary metastases than in primary tibia, with Gal3bp ($p > 0.05$) and Gal3 ($p = 0.08$) expression but not IL-6 expression being significantly upregulated ($p < 0.05$) (Figure 1D). However, in the murine primary tumor or pulmonary metastases we did not find any correlation between IL-6 and C1GALT1 (Figure S1B).

SFV vectors express Gal3 inhibitors that could block the binding of Gal3 to activated $CD8^+$ and $CD4^+$ T cells

Since we showed that Gal3 could be a potential target in osteosarcoma, we next generated SFV vectors expressing Gal3 inhibitors based on truncated forms of Gal3. These constructs included the Gal3 carboxy-terminal domain (SFV-Gal3-C) and its amino-terminal domain by itself (SFV-Gal3-N) or fused to the Gal3 peptide inhibitor C12 [28] (SFV-Gal3-N-C12). Gal3-C is a dominant-negative form of Gal3 that has the capacity to reduce tumor growth.[29] In the case of Gal3-N, we reasoned that it could interfere with the formation of Gal3 lattices, since this domain is important for Gal3 oligomerization.[30] Finally, fusion of Gal3-N with C12 could combine the inhibitory functions of both molecules. An additional construct expressed only the C12 peptide (SFV-C12) (Figure 2A). We confirmed the correct expression of each Gal3 inhibitor in cell extracts (CEs) and supernatants (SNs) of baby hamster kidney-21 (BHK) cells infected with the different SFV vectors by western blotting and immunofluorescence staining (Figures 2B and 2C). Since our aim was to use SFV vectors to treat osteosarcoma, we first confirmed that these vectors could infect osteosarcoma cells both *in vitro* and *in vivo*. *In vitro*, we were able to show that the K7M2 and MOS-J murine osteosarcoma cell lines expressed the SFV receptors and could be infected with SFV-Gal3-N-C12 with similar efficacy (Figures S2A–S2C). Using an SFV vector expressing luciferase (SFV-Luc), we also confirmed the capacity of SFV to infect K7M2 orthotopic tumors in mice *in vivo*. In this case, we observed high and transient expression of luciferase that peaked at days 2–6 and then decreased progressively until day 16, at which point it had decreased to background levels (Figure 2D). On the other hand, we also detected the Gal3-N-C12 inhibitor and SFV replicase in orthotopic K7M2 tumors after treatment with SFV-Gal3-N-C12 (Figure S2D).

As the binding of Gal3 to highly glycosylated receptors on the surface of $CD8^+$ T cells has been shown to induce T cell dysfunction,[31–33] we studied the capacity of our Gal3 inhibitors to block the binding of this protein to IL-10-activated $CD8^+$ and $CD4^+$ T cells. Notably, recombinant Gal3-N-C12 and Gal3-N efficiently blocked the binding of Gal3 to $CD8^+$ and $CD4^+$ T cells ($p < 0.0001$), with Gal3-N-C12 being slightly more efficient in $CD8^+$ T cells. The inhibition achieved with Gal3-N-C12 was similar (in $CD4^+$ T cells) or higher (in $CD8^+$ T cells) than that achieved with an anti-Gal3 antibody used as a positive control. However, Gal3-C had the opposite effect, increasing the binding of Gal3 (Figure 2E). In addition, since tumor-secreted Gal3 tends to bind to the

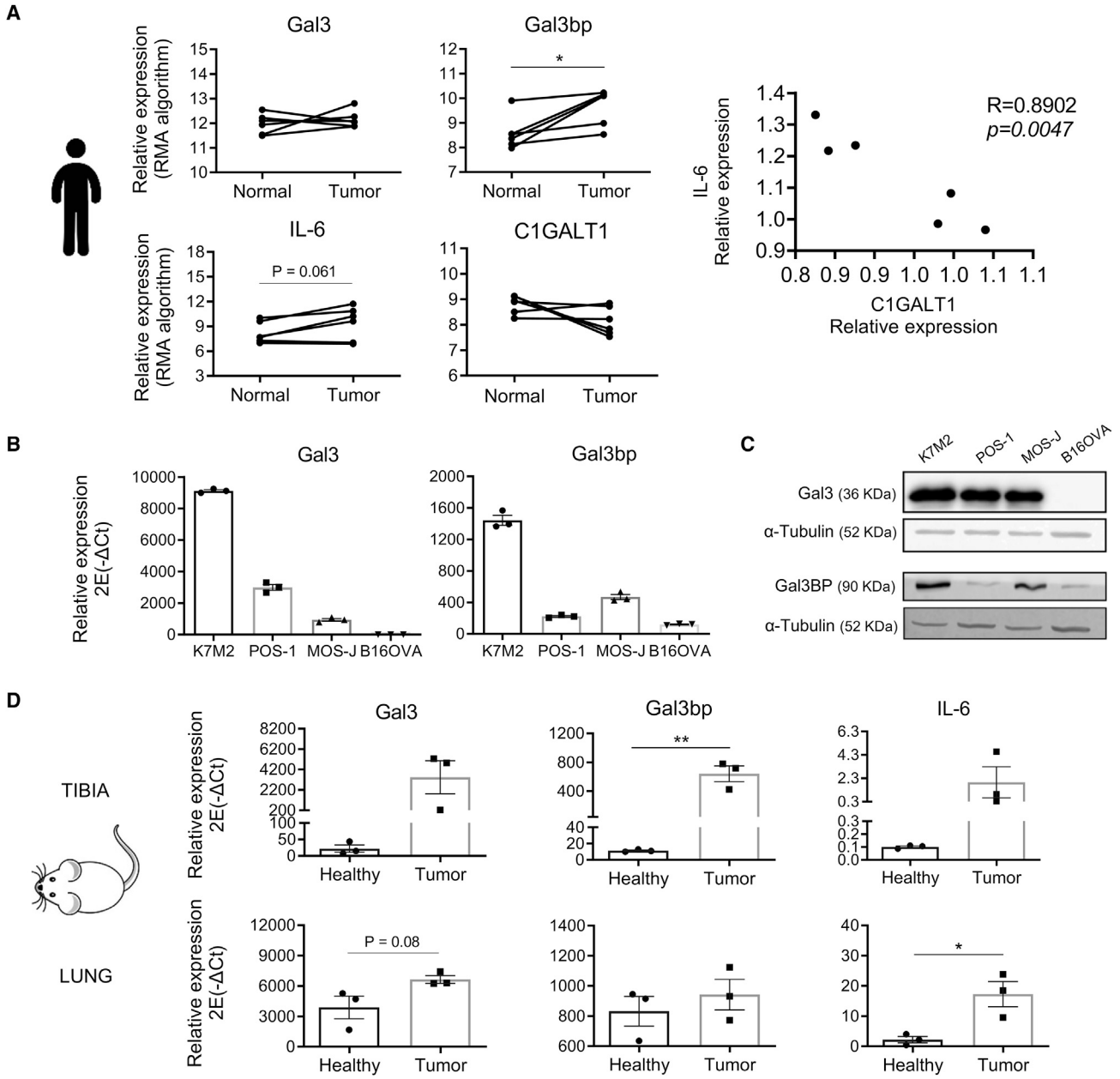

Figure 1. Expression of Gal3 and related genes in human patients and mouse models of osteosarcoma

(A) mRNA expression of Gal3 (*LGALS3*), Gal3bp (*LGALS3BP*), *IL-6*, and *C1GALT1* in tumor versus paired healthy samples from osteosarcoma patients (n = 6). The level of expression was determined using microarray analysis with the robust multiarray analysis (RMA) algorithm. Correlation of *IL-6* versus *C1GALT1* mRNA expression in tumor samples, $^{**}p < 0.01$ by Pearson's r. (B and C) mRNA (B) and protein (C) expression of Gal3 and Gal3bp in murine osteosarcoma cell lines (K7M2, MOS-J, and POS-1) and the murine melanoma cell line B16OVA determined by qRT-PCR (n = 3) and western blotting. (D) mRNA expression of Gal3, Gal3bp, and IL-6 in tibias and lungs representing healthy versus tumor tissue from orthotopic K7M2 tumor-bearing mice determined by qRT-PCR (n = 3). The data in (B) and (D) were calculated as 2E(−ΔCt) normalized to GAPDH × 10,000 and are presented as the mean ± SD. $^{*}p < 0.05$; $^{**}p < 0.01$; ns, not significant. Student's t test.

surface of effector $CD8^+$ T cells after activation,[24] we analyzed whether our Gal3 inhibitors could block Gal3 binding to $CD8^+$ and $CD4^+$ T cells expressing PD-1, which is a marker of T cell activation. The results showed that all recombinant inhibitors blocked the binding of Gal3 to the surface of $CD8^+PD1^+$ T cells ($p < 0.0001$) and that this inhibition was significantly higher with Gal3-N-C12 than with Gal3-N ($p < 0.01$), Gal3-C ($p < 0.01$), and the anti-Gal3 antibody used as a positive control ($p < 0.05$) (Figure 2F). The inhibitory effect on $CD4^+PD1^+$ T cells was very similar to that observed for $CD4^+$ T cells (Figure 2F). In addition,

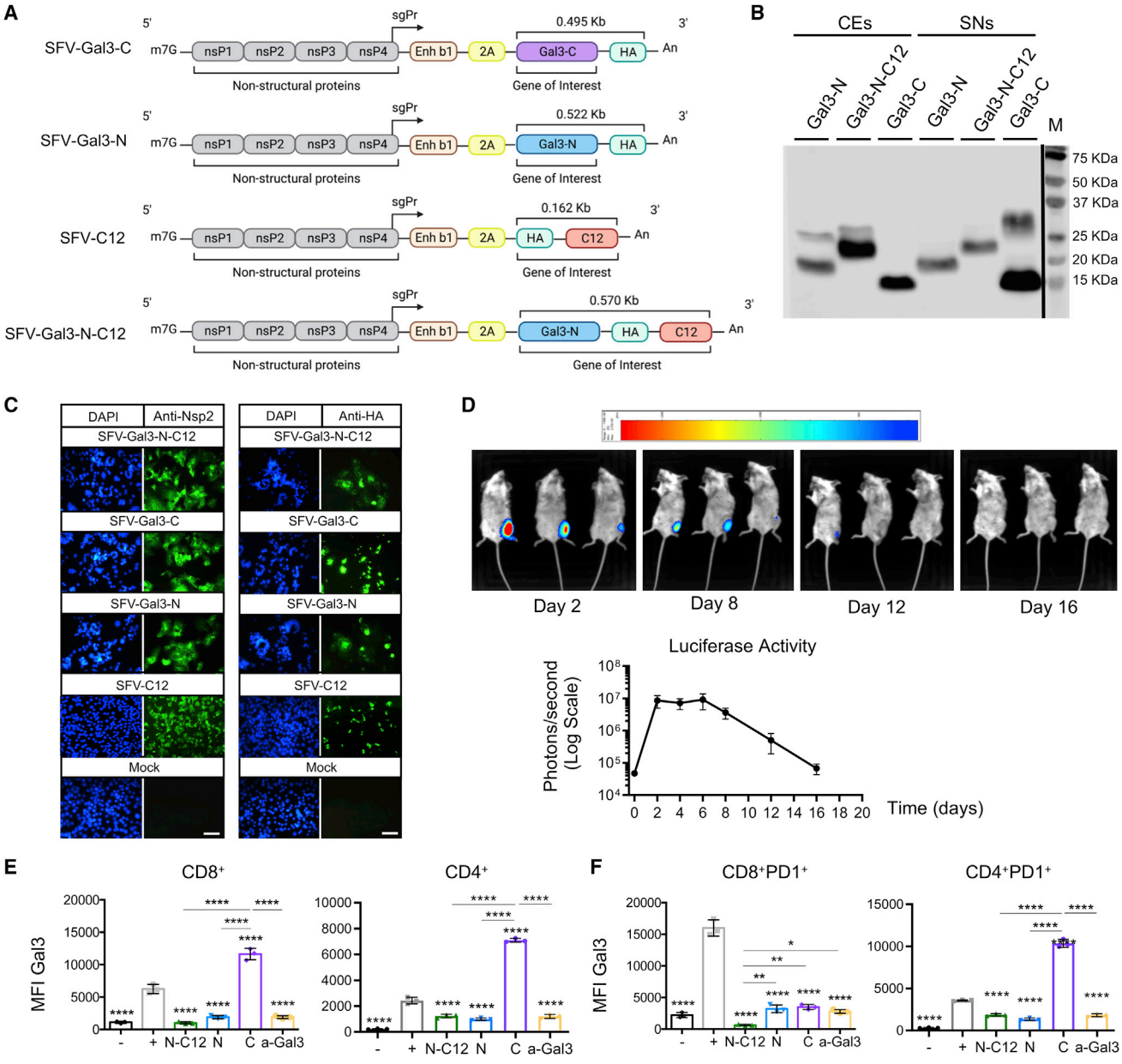

Figure 2. Characterization of SFV vectors expressing Gal3 inhibitors

(A) Diagrams of SFV vectors expressing Gal3 inhibitors: SFV-Gal3-C, SFV-Gal3-N, SFV-C12, and SFV-Gal3-N-C12. Constructs contained an SFV replicase sequence (composed of four nonstructural subunits [nsps]) followed by the viral subgenomic promoter (sgPr), a translation enhancer (b1) linked to the 2A FMDV protease fused in-frame to each Gal3 inhibitor sequences, and an HA tag. (B and C) Gal3 inhibitor expression in BHK-21 cells 24 h after infection with SFV vectors at an MOI of 20, as determined by western blot analysis of cell extracts (CEs) and supernatants (SNs) using an anti-HA antibody (B) and by immunofluorescence staining (C) using anti-nsp2 and anti-HA antibodies. Cell nuclei were stained with DAPI (magnification, 200×; scale bar, 100 μm). (D) Luciferase activity was determined in orthotopic K7M2 tumor-bearing mice at the indicated times after intratumoral injection of 1×10^8 VPs SFV-Luc; signal is measured in photons/s. Data represent the mean ± SD (n = 3). Images of luciferase expression in mice are shown. (E and F) Inhibition of Gal3 binding to activated T cells. $CD8^+$ and $CD4^+$ T cells activated with anti-CD3 and anti-CD28 antibodies and incubated with IL-10 were treated with the indicated recombinant Gal3 inhibitors at 50 μM ($CD8^+$) or 25 μM ($CD4^+$), with an anti-Gal3 antibody (a-Gal3) at 20 μg/mL ($CD8^+$) or 10 μg/mL ($CD4^+$) in the presence of 5 μg/mL recombinant Gal3 (+) for 30 min ($CD8^+$) or 48 h ($CD4^+$). Cells incubated without inhibitors and Gal3 indicated by (–). The binding of Gal3 was determined by flow-cytometric measurement of the mean fluorescence intensity (MFI) of Gal3 on total $CD8^+$ and $CD4^+$ T cells (E) or in $CD8^+PD1^+$ and $CD4^+PD1^+$ T cells (F). Data are presented as the mean ± SD (n = 3). *p < 0.05, **p < 0.01, ***p < 0.001, ****p < 0.0001; one-way ANOVA. N, Gal3-N; C, Gal3C; N-C12, Gal3-N-C12.

Gal-N-C12 was able to induce decreases in the percentages of $CD4^+PD1^+$ and $CD4^+CD25^+$ T cells compared with the anti-Gal3 antibody ($p < 0.0001$, $p < 0.0001$) and other Gal3 inhibitors tested (Figure 2E).

SFV-Gal3-N-C12 displays a robust antiosteosarcoma effect *in vitro* and *in vivo*

Before testing the antitumor effect of SFV vectors expressing Gal3 inhibitors *in vivo*, we evaluated the cytopathic effects of these vectors in two osteosarcoma cell lines *in vitro*. We observed that all SFV vectors were able to kill murine osteosarcoma cells at 24 and 72 h after infection and that this effect was greater in K7M2 cells than in MOS-J cells, being dependent on multiplicity of infection (MOI) in both cell lines. In both cell lines, SFV-Gal3-N-C12 displayed the best half-maximal inhibitory concentration (IC_{50}) (Figure S3A). To estimate the therapeutic effectiveness of our strategy, we evaluated the antitumor effect of SFV vectors administered to two orthotopic models of murine osteosarcoma by intratumoral injection. Both K7M2 tumors and MOS-J tumors were injected 7 days after intratibial injection of tumor cells with 10^8 viral particles (VPs) of SFV vectors, as shown in Figure 3A. We observed that SFV-Gal3-N-C12 treatment significantly delayed tumor growth in comparison with treatment with the other vectors or PBS (Figures 3B and 3C). For example, on day 15 post treatment, SFV-Gal3-N-C12-injected mice showed tumors with an average size of 132.10 ± 20.25 mm^2, which was approximately half the size of the tumors in mice treated with PBS (245.45 ± 32.75 mm^2), SFV-Luc (212.54 ± 50.09 mm^2), or SFV-Gal3-C (219.36 ± 65.47 mm^2). SFV-Gal3-N also produced a significant antitumor effect (147.61 ± 26.10 mm^2), although this effect was maintained for a shorter time in most tumors (Figure 3B). We confirmed the high antitumor efficacy of SFV-Gal3-N-C12 in a second experiment that included SFV-C12, although this vector did not produce a significant antitumor effect (Figure S4A). Importantly, treatment of K7M2 tumor-bearing mice with SFV-Gal3-N-C12 significantly increased the median survival time of the treated mice (PBS: 24 days; SFV-Luc: 22.5 days; SFV-C12: 28 days; SFV-Gal3-N-C12: 85 days; SFV-Gal3-N: 26 days; SFV-Gal3-C: 24 days). Furthermore, treatment with SFV-Gal3-N-C12 led to a higher rate of long-term survivor mice (47%) in comparison with the other treatments. The rates for the other treatments were as follows: PBS (6%, $p < 0.001$), SFV-Luc (20%, $p < 0.05$), SFV-C12 (0%, $p < 0.05$), SFV-Gal3-N (5%, $p < 0.01$), and SFV-Gal3-C (0%, $p < 0.001$) (Figure 3D, pooled data from both experiments). Monitoring of mouse weight showed normal weight gain among the treatments, suggesting that the injection of SFV vectors did not produce toxicity (Figures S4B and S4C). However, only 25% of long-term survivors showed protection after rechallenge with the same tumor cells ($p = 0.09$; Figure 3E). SFV-Gal3-N-C12 also showed antitumor effects in MOS-J tumor-bearing animals, significantly controlling tumor growth (Figures 3F and S4D) and prolonging survival (30% long-term survivors) in comparison with PBS ($p < 0.05$) or SFV-Luc ($p < 0.05$) (Figure 3G). In this model, 100% of long-term survivors showed protection after rechallenge with MOS-J cells, which was significantly different from the lack of protection in naive mice ($p < 0.05$) (Figure 3H).

Treatment with SFV-Gal3-N-C12 partially reduces spontaneous osteosarcoma pulmonary metastases

Since metastasis constitutes the main cause of death in pediatric patients with osteosarcoma, we also investigated the antimetastatic effect of SFV vectors expressing Gal3 inhibitors. We conducted anatomopathological analyses of the lungs of K7M2 tumor-bearing mice treated with SFV vectors in the efficacy study presented in Figure 3B; the lungs were evaluated at the time of sacrifice/death. SFV-Gal3-N-C12-treated mice showed fewer metastases than mice treated with other SFV vectors (Figure 4A). Pulmonary metastases were observed in 32% of the total lungs in the SFV-Gal3-N-C12-treated group, whereas SFV-Gal3-C, SFV-Gal3-N, and SFV-Luc showed milder antimetastatic effects, with metastases observed in 50%, 69%, and 60% of the total lungs in each group, respectively. In contrast, neither SFV-C12 nor PBS reduced pulmonary metastases, with metastases observed in 88% of the total lungs in both groups (Figure 4A). MicroCT analysis, performed on day 14 post treatment, revealed a partial antimetastatic effect of SFV-Gal3-N-C12 ($p > 0.05$) compared with PBS or SFV-Luc ($n = 3$). The average healthy lung parenchymal area was higher in the SFV-Gal3-N-C12 group (245 ± 96.13 mm^2) than in the SFV-Luc (178 ± 36.98 mm^2) and PBS (148 ± 65.45 mm^2) groups, although it did not reach the levels observed in healthy mice (305 ± 13.94 mm^2) (Figure 4B). More interestingly, analysis of RNA sequencing (RNA-seq) data from primary K7M2 tumors collected on day 14 post treatment revealed downregulation of genes previously reported to be prometastatic in osteosarcoma[34] in the SFV-Gal3-N-C12 group compared with the SFV-Luc and PBS groups ($p < 0.01$; Figure 4C). Some of the prometastatic genes that were downregulated after treatment with SFV-Gal3-N-C12 included *EZR*, *TGFB1*, *HIF1a*, *CD276*, *EGFR*, *CCN1*, and *ITGB4*, which are involved in the hypoxia-induced response, immunosuppression, tumor growth, or migration and invasion (Figure 4D).

SFV-Gal3-N-C12 remodels the immune landscape in primary osteosarcoma tumors and pulmonary metastases

Since both Gal3 and SFV vectors can induce changes in the tumor microenvironment that can affect immune responses,[35–37] we next investigated the impact of SFV-Gal3-N-C12 on antitumor immune responses. For this study, we used mice bearing K7M2 tumors that were sacrificed 14–17 days after vector treatment. SFV-Gal3-N-C12-treated mice showed a slight increase in the number of $CD3^+$ cells in the primary tumor compared with PBS- or SFV-Luc-treated mice, although this increase did not reach significance ($p = 0.06$) (Figure 5A). Furthermore, transcriptomic analysis of primary tumors showed differences in the relative abundances of several immune cell populations when comparing the PBS, SFV-Gal3-N-C12, and SFV-Luc treatments (Figure 5B). Interestingly, SFV-Gal3-N-C12 increased the abundance of pDCs compared with SFV-Luc ($p < 0.05$). SFV-Gal3-N-C12 also increased natural killer (NK) cell ($p < 0.0001$) and type 1 conventional dendritic cell (cDC1) ($p < 0.001$) levels and decreased the abundances of M1 ($p < 0.01$) and M2 ($p < 0.01$) macrophages in comparison with PBS. In contrast, SFV-Luc induced only a reduction in M2 macrophages in treated tumors compared with PBS ($p < 0.05$) (Figure 5C). Of relevance, we

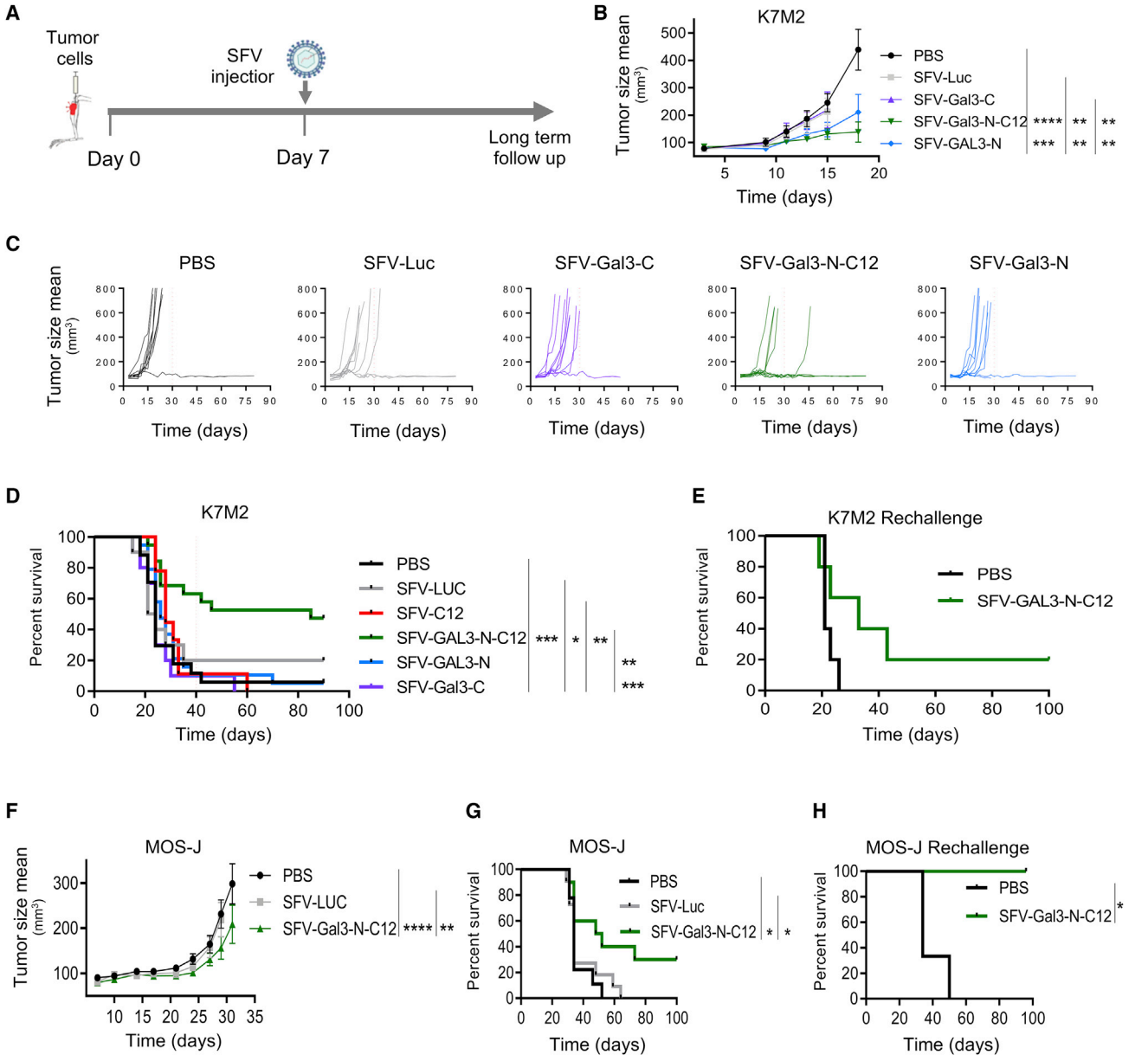

Figure 3. Evaluation of the antitumor effect of SFV vectors expressing Gal3 inhibitors in osteosarcoma

(A) Treatment schedule for orthotopic osteosarcoma mouse models. Tumor cells were injected intratibially on day 0. The tumors were treated with 1×10^8 VPs SFV on day 7, and tumor size and survival were monitored. (B) K7M2 tumor growth in mice treated with the indicated vectors (n = 10) or PBS (n = 9). A representative experiment is shown of two experiments with similar results. Data are shown as the mean ± SD. *p < 0.05, **p < 0.01, ***p < 0.001, ****p < 0.0001; extra sum-of-squares F test. (C) Individual tumor growth of the mice presented in (B). Discontinuous red line indicates time when control mice developed tumors >400 mm^2. (D) Kaplan-Meier survival plot of the mice described in (A). The graph corresponds to pooled data from two experiments using SFV-Gal3-C (n = 10), SFV-Gal3-N (n = 19), SFV-Gal3-N-C12 (n = 19), SFV-C12 (n = 9), SFV-Luc (n = 10), and PBS (n = 17). *p < 0.05, **p < 0.01, ***p < 0.001; log-rank test. (E) Kaplan-Meier survival curves of cured K7M2 tumor-bearing mice rechallenged with K7M2 cells (n = 5). p > 0.05 (not significant); log-rank test. (F) Tumor growth evaluation of MOS-J tumor-bearing mice treated as described in (A) with the indicated vectors (n = 9–10). Data are shown as the mean ± SD. *p < 0.05, **p < 0.01, ***p < 0.001, ****p < 0.0001; extra sum-of-squares F test. (G) Kaplan-Meier survival plot of the MOS-J tumor-bearing mice described in (A). *p < 0.05, log-rank test. (H) Kaplan-Meier survival plot of cured MOS-J tumor-bearing mice rechallenged with MOS-J cells (n = 3). *p < 0.05, log-rank test.

A

Treatment	Bone tumor	Lung metastasis	Survivors
PBS	82 % (14/17)	88 % (15/17)	6 %(1/17)
SFV-LUC	80 % (8/10)	60 % (6/10)	20 % (2/10)
SFV-Gal3-C	90 % (9/10)	50 % (5/10)	0 % (0/10)
SFV-Gal3-N	68 % (13/19)	68 % (13/19)	5 % (1/19)
SFV-Gal3-N-C12	42% (8/19)	32 % (6/19)	47 % (9/19)
SFV-C12	89% (8/9)	89 % (8/9)	0% (0/9)

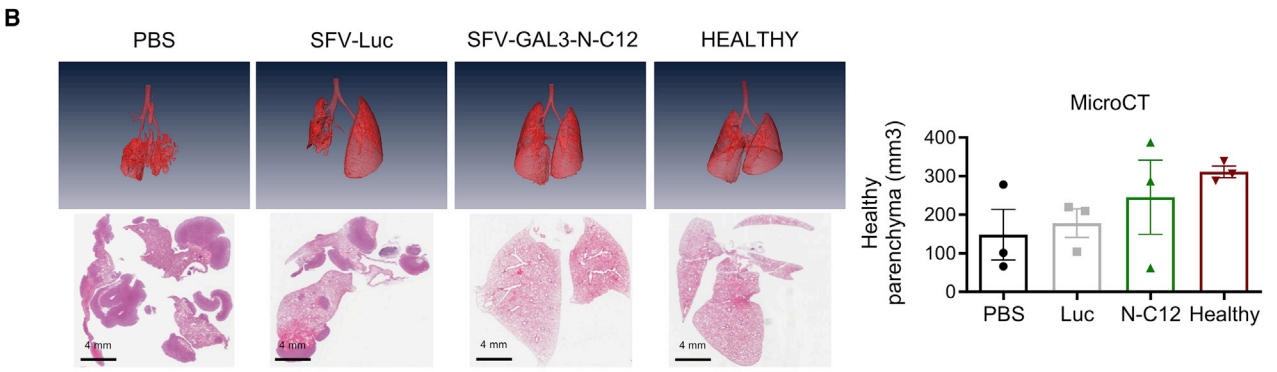

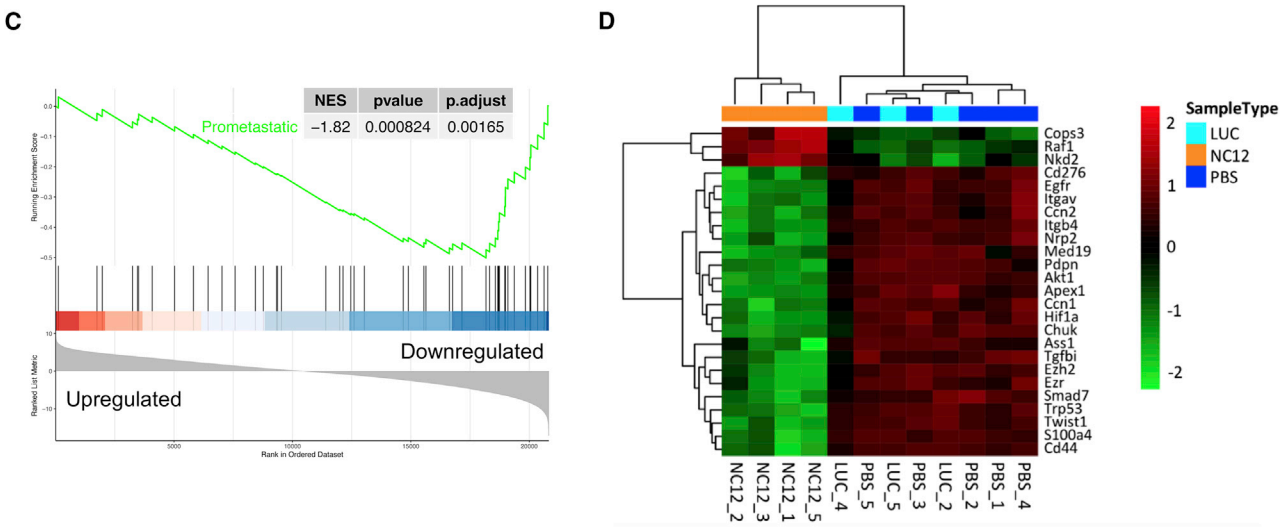

Figure 4. Assessment of the antimetastatic effect of SFV vectors in an orthotopic K7M2 osteosarcoma mouse model

(A) Summary table for survival, presence of metastases, and presence of bone tumors from two pooled experiments evaluating K7M2 tumor-bearing mice treated with the indicated SFV vectors or PBS. (B) Analysis of lung metastases. K7M2 tumor-bearing mice were analyzed on day 15 after treatment with PBS, SFV-Luc, or SFV-Gal3-N-C12, and healthy mice without tumors were used as controls. MicroCT analysis (upper images) and H&E staining (lower images) of lung tissue samples from one representative mouse in each group (magnification, 20×; scale bar, 4 mm). Quantification of the volume of the healthy lung parenchyma in all mice in the different treatment groups. Data are presented as the mean ± SD (n = 3, each group). $p > 0.05$ (not significant); one-way ANOVA. (C and D) Analysis of gene expression by RNA-seq. Mice bearing K7M2 tumors were treated with SFV-Gal3-N-C12 (NC12, n = 4), SFV-Luc (LUC, n = 3), or PBS (n = 5) as described in Figure 3A. On day 14 the mice were sacrificed, and total RNA was extracted from the tumors for sequencing. (C) Upon gene set enrichment analysis, an enriched gene set of prometastatic genes involved in osteosarcoma pathology was downregulated in the SFV-Gal3-N-C12 (NC12) group compared with the SFV-Luc (LUC) group at nominal $p < 0.01$ and false discovery rate (FDR) < 0.05. Normalized enrichment score (NES), −1.82; $^{**}p_{adjusted} < 0.01$. (D) A heatmap and hierarchical clustering representing the differential expression of the most significant prometastatic genes between the treatment groups.

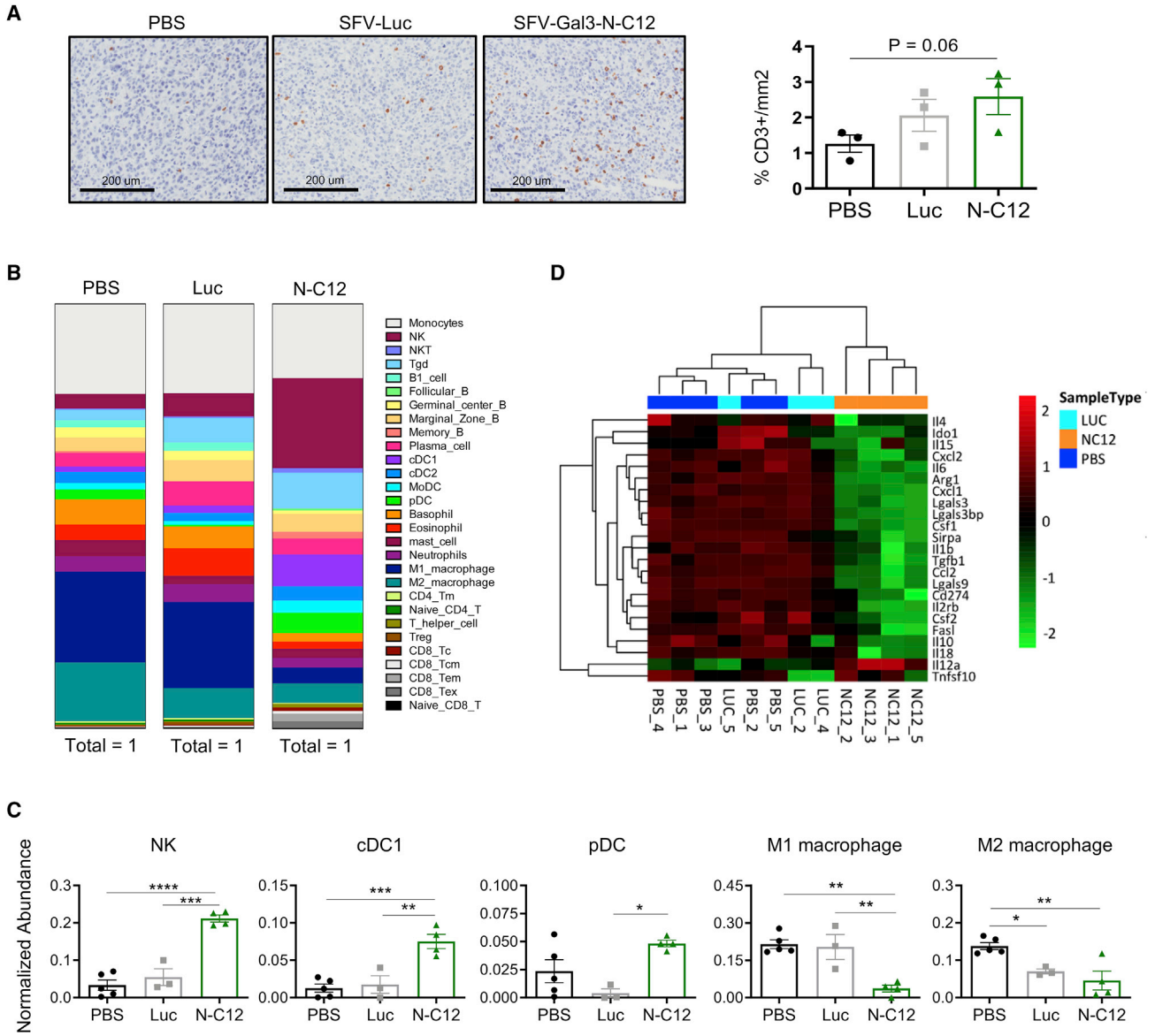

Figure 5. Analysis of immune cell populations in primary K7M2 tumors after treatment with SFV vectors by immunohistochemistry and RNA-seq

(A) Immunohistochemistry (IHC) analysis of $CD3^+$ T cells in primary osteosarcoma tumors from mice sacrificed at 14–17 days after intratumoral treatment with the indicated vectors or PBS. Representative IHC images are shown. Quantification of $CD3^+$ T cells presented as the percentage of cells stained positive for CD3 in IHC images (magnification, 400×; scale bar, 200 μm). $CD3^+$ T cells were counted in five different fields in each sample, and the mean was used to perform statistical analysis. Data are shown as the mean ± SD (n = 3). $p > 0.05$ (not significant); one-way ANOVA. (B) Relative abundances (in percentages) of 29 different immune cell populations determined by analysis of RNA-seq data for primary tumors from K7M2 tumor-bearing mice obtained as described in Figure 4C with the online tool ImmuCellAI-mouse. The abundance of each population was normalized by considering 1 to be the total (100%) population abundance. (C) Normalized abundances of natural killer (NK) cells, type 1 dendritic cells (cDC1s), plasmacytoid dendritic cells (pDCs), M1 macrophages, and M2 macrophages. Data are shown as the mean ± SD (n = 3–5). *$p < 0.05$, **$p < 0.01$, ***$p < 0.001$, ****$p < 0.0001$; one-way ANOVA. (D) Heatmap representing the differential expression and hierarchical clustering of the most significant immunomodulatory genes between treatment groups. NC12, SFV-Gal3-N-C12; LUC, SFV-Luc.

observed downregulation of the expression of several genes encoding immunomodulatory molecules. The genes downregulated after treatment with SFV-Gal3-N-C12 included the immunosuppressive molecules Gal3, Gal3bp, IL-4, IL-10, Ido, Arg-1, Tgf-b, and Gal9, as well as gene sets related to different pathways involved in immunosuppression (Figures 5D and S5A). On the other hand, some important immunostimulatory genes, such as IL-12 and TRAIL (*TNFSF10*), were upregulated by SFV-Gal3-N-C12, suggesting that SFV-Gal3-N-C12 treatment could disrupt the immunosuppressive environment inside osteosarcoma tumors and remodel the immune landscape.

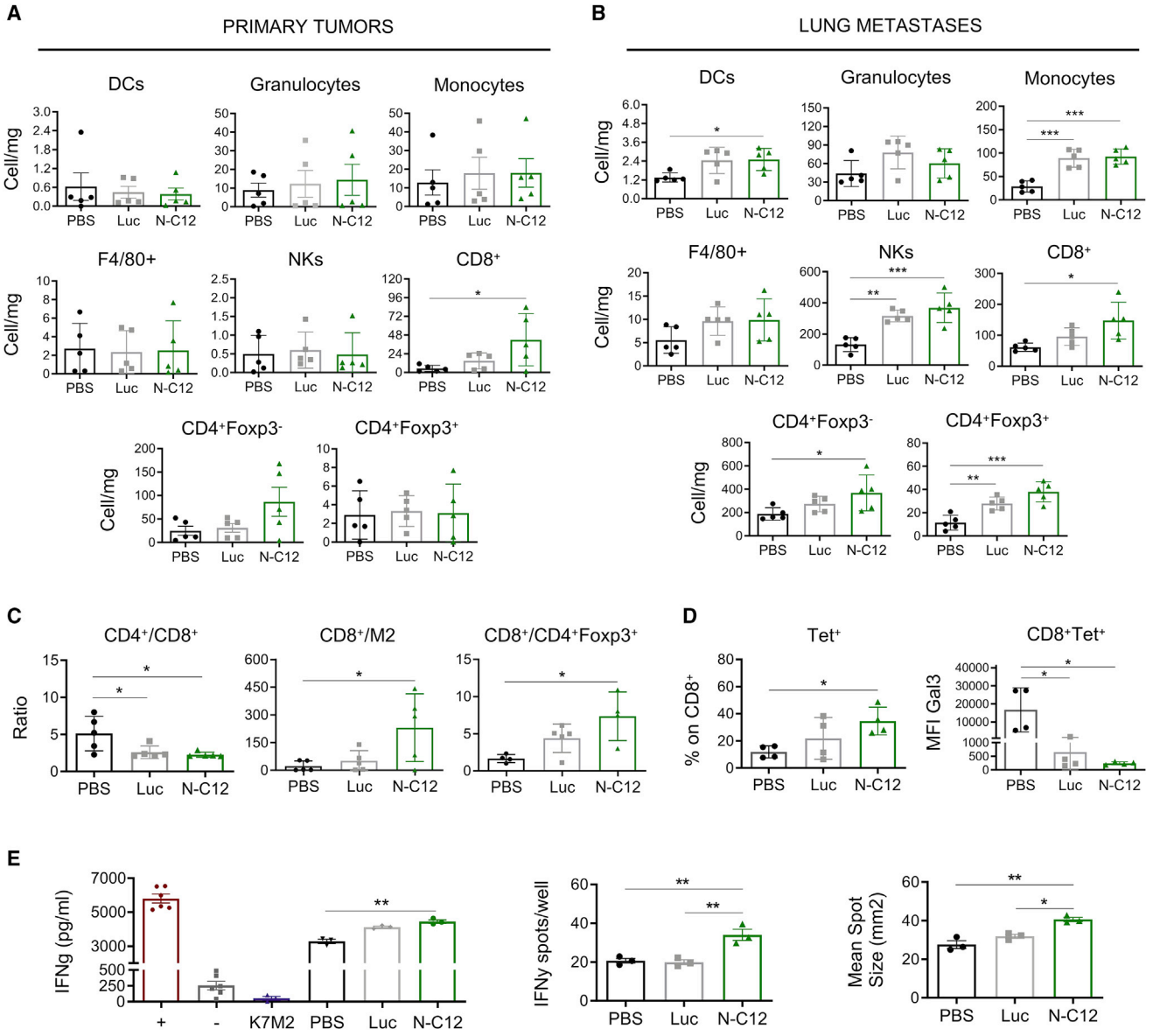

Figure 6. Characterization of the tumor microenvironment of K7M2 tumors after treatment with SFV vectors

(A and B) Flow-cytometric analyses of different immune cell populations in primary K7M2 tumors (tibias) (A) and lung metastases (B) on day 3 after treatment with PBS, SFV-Gal3-N-C12 (N-C12), or SFV-Luc (Luc). Data are shown as the number of cells/mg tissue and as the mean ± SD (n = 5). *p < 0.05, **p < 0.01, ***p < 0.001; one-way ANOVA. (C) Ratios of $CD4^+/CD8^+$ T cells, $CD8^+$ T cells/M2 macrophages, and $CD8^+/CD4^+Foxp3^+$ T cells in the tumor samples analyzed in (A). Data are shown as the mean ± SD (n = 5). *p < 0.05; one-way ANOVA. (D) Gp70 tetramer (Tet^+) staining (%) of the $CD8^+$ T cell population (%) and surface expression of Gal3 in the $CD8^+Tet^+$ T cell population (MFI) in K7M2 tumors on day 14 after treatment with the indicated vectors. Data are shown as the mean ± SD (n = 4). *p < 0.05, **p < 0.01, ***p < 0.001; one-way ANOVA. (E) IFN-γ production in TILs isolated from K7M2 primary tumors on day 14 after treatment with the indicated SFV vectors. IFN-γ levels were measured by ELISA, and IFN-γ spot numbers and IFN-γ mean spot sizes were measured by ELISPOT. Data are shown as the mean ± SD (n = 3). *p < 0.05, **p < 0.01; one-way ANOVA. +, splenocytes plus mitogen; −, only splenocytes; K7M2, only K7M2 cells.

To confirm the implications for the immune system, specifically the antitumor response induced by SFV-Gal3-N-C12 against K7M2 osteosarcomas, we analyzed immune cell populations at different times after treatment by flow cytometry (Figure S6A). On day 3 after treatment, both $CD8^+$ T cells and conventional $CD4^+Foxp3^-$ T cells were increased in primary tumors from mice treated with SFV-Gal3-N-C12 compared with those treated with SFV-Luc or PBS (Figure 6A). Interestingly, evaluation of the same populations in pulmonary metastases at the same time point showed significant increases in $CD8^+$ T cells, $CD4^+$ ($Foxp3^+$ and $Foxp3^-$) T cells, dendritic cells

(DCs), monocytes, and NK cells in mice treated with SFV-Gal3-N-C12 and to a lesser extent in those treated with SFV-Luc compared with those treated with PBS (Figure 6B). Treatment with SFV-Gal3-N-C12 also induced increases in the $CD8^+/CD4^+Foxp3^+$ T cells ($p < 0.05$) and $CD8^+$ T cell/M2 macrophage ($p < 0.05$) ratios in primary tumors, as well as a decrease in the $CD4^+/CD8^+$ T cell ratio ($p < 0.05$) in both primary tumors and pulmonary metastases, in comparison with treatment with PBS (Figures 6C and S7A). These data indicated an early proinflammatory response induced by SFV-Gal3-N-C12. However, on day 7 after treatment, the responses were more attenuated, with no significant differences in myeloid or lymphoid populations in primary tumors found among the groups; in contrast, in lung metastases, DCs and monocytes were still significantly elevated (Figure S7B). However, despite the lower abundance of $CD8^+$ T cells at times later than 3 days post treatment, we observed an increase in the percentage of tumor-specific $CD8^+$ T cells ($CD8^{Tet+}$) in the primary tumors of SFV-Gal3-N-C12-treated mice ($p < 0.05$) compared with those of PBS-treated mice at 14 days (Figure 6D). These cells also showed less Gal3 expressed on the surface, along with increased secretion of IFN-γ upon stimulation with tumor cells (Figure 6E). All of these data suggested that SFV-Gal3-N-C12 could trigger a rapid immune response led by early increases in the $CD8^+$ and $CD4^+Foxp3^-$ T cell populations, generating a strong specific antitumor immune response over time.

Treatment with SFV-Gal3-N-C12 prevents tumor-infiltrating $CD8^+$ T cells from acquiring an exhausted phenotype in the context of K7M2 tumors

To further elucidate the phenotypic changes that may explain the potent antitumor immune response triggered by SFV-Gal3-N-C12, we analyzed the expression of the activation/exhaustion markers PD-1, LAG-3, and TIM3 in $CD8^+$ and $CD4^+$ T cells from primary tumors at two different time points after treatment. On day 3, $CD8^+$ T cells showed no differences in the expression of PD-1 or LAG3 among treatments. However, TIM3 expression was increased in these cells after treatment with SFV-Luc ($p < 0.01$) or SFV-Gal3-N-C12 ($p < 0.05$) compared with PBS treatment, although these increases were lost on day 7 (Figure 7A). When analyzing the percentage of $CD8^+$ T cells coexpressing several exhaustion markers, we observed that the percentage of $CD8^+PD1^+LAG3^+$ T cells was greater in the SFV-Gal3-N-C12 group on day 3 (Figure 7B). Interestingly, on day 7, $CD8^+$ T cells coexpressing PD1 and/or LAG3 and/or TIM3 from SFV-Gal3-N-C12-treated tumors remained almost unchanged, whereas these populations were increased in the SFV-Luc group. Notably, the percentage of $CD8^+$ T cells with a highly exhausted phenotype ($PD1^+LAG3^+TIM3^+$)[38] was 4.97% ± 2.68% in the SFV-Luc group compared with 0.56% ± 0.51% in the SFV-Gal3-N-C12 group (Figure 7B). In summary, these results suggested that whereas the SFV vector could trigger the activation of $CD8^+$ T cells, Gal3-N-C12 expression could prevent exhaustion. On the other hand, similar results, albeit with a weaker effect, were observed for $CD4^+$ T cells specifically for both the individual expression of PD1, LAG3, and TIM3 (Figure 7C) and the percentage of cells with an exhausted phenotype (Figure 7D).

SFV-Gal3-N-C12 decreases the accumulation of immune cell populations upregulated in osteosarcoma pulmonary metastases

Since the modulation of immune cell populations in primary tumors can have an effect on metastasis formation, we studied the presence of $CD4^+PD1^+$ and $CD4^+CD25^+$ T cells in both primary tumors and lung metastases. These populations have been described to have positive correlations with the number and progression stage of osteosarcoma pulmonary metastases in patients.[39,40] We also studied the presence of $CD8^+$ T cells expressing Gal3 on the surface, as Gal3 can cause dysfunction in these cells, leading to a failure to control tumor invasion. Interestingly, on day 14 after treatment, we observed reductions in the percentages of $CD4^+PD1^+$ ($p < 0.05$), $CD4^+CD25^+$ ($p < 0.05$), $CD4^+Gal3^+$ ($p > 0.05$), and $CD8^+Gal3^+$ ($p < 0.05$) T cells in the primary tumors of mice treated with SFV-Gal3-N-C12 compared with those of mice treated with PBS. Moreover, SFV-Luc also decreased $CD4^+Gal3^+$ and $CD8^+Gal3^+$ T cells to the same levels as SFV-Gal3-N-C12 (Figure 8A). Similar results were obtained when these populations were analyzed in the pulmonary metastases of the same animals. Nevertheless, in these metastases, SFV-Gal3-N-C12 treatment decreased the percentages of $CD4^+PD1^+$, $CD4^+CD25^+$, and $CD4^+Gal3^+$ T cells in comparison with either PBS or SFV-Luc treatment (Figure 8B). In primary tumors, the $CD4^+PD1^+$ and $CD4^+CD25^+$ T cell populations from PBS-treated mice had more Gal3 expressed on the surface than the same populations from mice treated with SFV-Gal3-N-C12 ($p < 0.05$) or SFV-Luc ($p < 0.05$) (Figure S8A). However, in pulmonary metastases, only SFV-Gal3-N-C12 was able to decrease the amount of Gal3 expressed on the surface of these populations (Figure S8B). Treatment with both SFV vectors also reduced the accumulation of $CD4^+Foxp3^-CD25^{hi}$ T cells in primary tumors but not in pulmonary metastases compared with PBS treatment (Figures 8A and 8B). This population may have an essential role in establishing immunosuppression, since these cells express higher levels of the immunosuppressive cytokine IL-10 than the $CD4^+Foxp3^+CD25^{hi}$ population (Figure S8C). These results showed that whereas both SFV vectors could reduce the expansion of $CD4^+PD1^+$ and $CD4^+CD25^+$ T cell populations in primary tumors and partially control tumor invasion, complementation with a Gal3-N-C12 inhibitor also reduced the accumulation of these immune cell populations in pulmonary metastases.

DISCUSSION

Osteosarcomas that do not respond to therapy or present with metastasis constitute an unmet clinical need. In this context, the use of SFV-based vectors poses an alternative approach for treating this disease. In fact, a previous study showed the feasibility of using an oncolytic SFV vector expressing GFP to treat a highly aggressive orthotopic osteosarcoma model.[11] Although this propagating-competent virus displayed some efficacy, it failed to generate long-term survivors, highlighting the need to enhance the efficacy of SFV vectors. Currently, arming an oncolytic virus with immunomodulatory ligands can improve the antisarcoma effect of other oncolytic viruses.[41,42] There is a plethora of potential targets available to be used; however, human osteosarcoma samples express high levels of

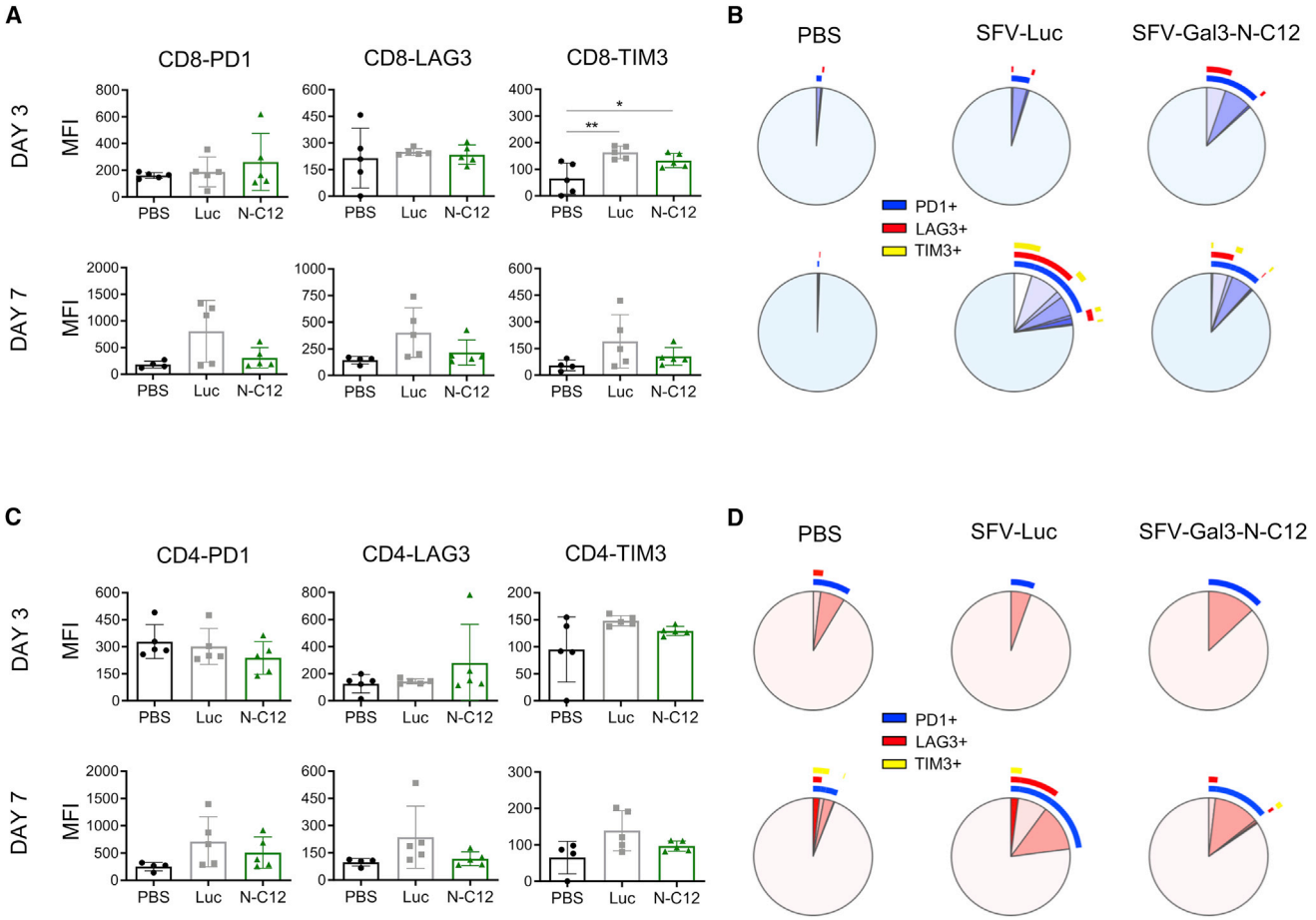

Figure 7. Analysis of exhaustion markers expressed by tumor-infiltrating lymphocytes in K7M2 tumors after treatment with SFV vectors

(A) Expression of PD1, LAG3, or TIM3 (MFI) in $CD8^+$ T cells from K7M2 tumors on day 3 and day 7 after treatment with PBS, SFV-Luc (LUC), or SFV-Gal3-N-C12 (N-C12). Data are shown as the mean ± SD (n = 5, each group). *$p < 0.05$, **$p < 0.01$; one-way ANOVA. (B) Pie charts showing the percentage of $CD8^+$ T cells coexpressing the activation/exhaustion markers PD1, LAG3, and TIM3. (C) Same analysis as in (A) performed with tumor-infiltrating $CD4^+$ T cells. Data are shown as the mean ± SD (n = 5, each group). $p > 0.05$ (not significant); one-way ANOVA. (D) Pie charts showing the percentage of $CD4^+$ T cells coexpressing the activation/exhaustion markers PD1, LAG3, and TIM3.

Gal3,[13] and its silencing in cultured human osteosarcoma cells was shown to decrease cell migration and invasion capabilities.[17] Importantly, Gal3 acts as a negative regulator of the innate and adaptive immune systems, thereby diminishing the immune response against the tumor, which underscores the potential of this protein as a therapeutic target. It seems that the highly immunosuppressive environment inside the tumor produces therapeutic failure in nonresponders and metastatic patients mainly triggered by a high concentration of IL-6, among other protumoral cytokines.[27,43–45] Along this line, the binding of Gal3bp (the main ligand of Gal3) secreted by neuroblastoma cells to Gal3 expressed on the surface of bone marrow mesenchymal stem cells (BMMSCs) and monocytes was shown to induce the expression of IL-6 via the Gal-3BP/Gal-3/Ras/MEK/ERK signaling pathway and lead to immunosuppression.[22] We observed notable overexpression of Gal3bp but a modest increase in IL-6 expression in primary tumor samples from osteosarcoma patients. However, primary tumors from an orthotopic osteosarcoma mouse model showed increases in the expression of Gal3, Gal3bp, and IL-6 compared with healthy paired samples. The slight correlation between the levels of Gal3bp and IL-6 in human samples suggested that tumor-secreted Gal3bp could trigger the induction of IL-6, perhaps by binding to Gal3 on the surface of BMMSCs. The inhibition of Gal3bp binding to Gal3 might reduce the immunosuppressive environment inside osteosarcoma tumors to favor tumor eradication by the immune system. Nevertheless, further analyses are needed to fully understand the relationship among these three proteins in the context of osteosarcoma. Despite the rather small difference we observed in Gal3 levels in human samples perhaps due to the small samples (n = 6), it has been previously described that Gal3 is significantly upregulated in osteosarcoma patients both in serum and in tumor tissues, which also correlated with the Enneking stage of cancer and the occurrence of metastasis.[13] Of note in our samples,

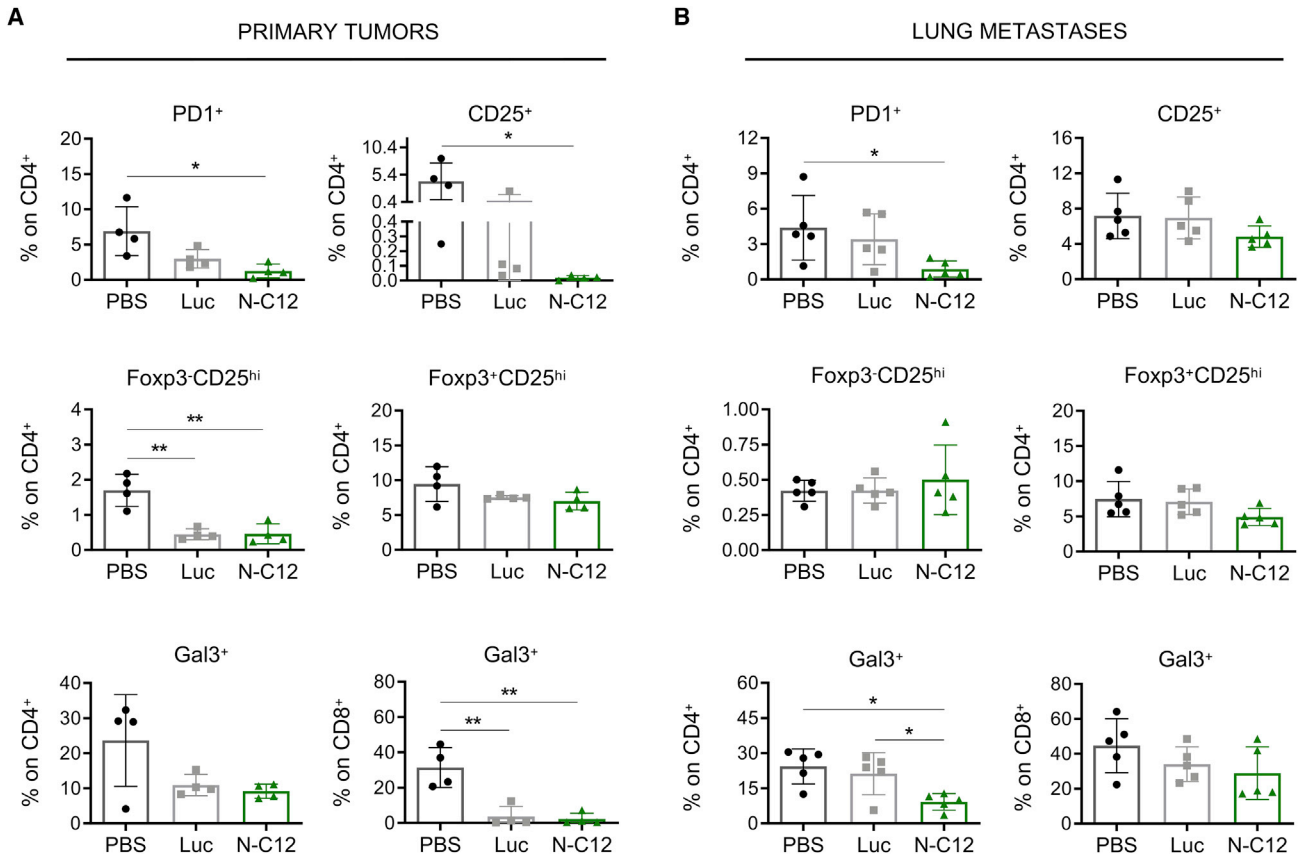

Figure 8. Modulation of immune cell populations involved in pulmonary osteosarcoma metastases

Flow-cytometric analyses of $CD4^+$ or $CD8^+$ T cells expressing PD1, Foxp3, CD25, and/or Gal3 in the primary tumors (tibias) (A) and pulmonary metastases (B) of mice bearing K7M2 tumors on day 14 after treatment with PBS, SFV-Gal3-N-C12 (N-C12), or SFV-Luc (Luc). Data are shown as the mean percentage ± SD of the total $CD4^+$ or $CD8^+$ T cells (n = 5). *p < 0.05, **p < 0.01, ***p < 0.001; one-way ANOVA.

Gal3bp was significantly increased in tumor tissue compared with the normal one. These data together with our observations underscore the potential of Gal3 as a therapeutic target in osteosarcoma.

A single dose of SFV-Gal3-N-C12 showed remarkable inhibition of tumor growth and led to long-term survival in both osteosarcoma models tested. A modest antitumor effect was also observed with SFV vectors expressing either Gal3-N or C12, indicating that both components of Gal3-N-C12 could contribute to the inhibition of tumor growth. Additionally, treatment with SFV-Gal3-N-C12 led to a robust antimetastatic effect that was accompanied by a reduction in the $CD4^+PD\text{-}1^+$ T cell population, which has been reported to favor pulmonary metastasis in osteosarcoma patients and correlate with more advanced stages of this disease.[39]

The mechanism of action underlying the therapeutic effect of this vector can be attributed to several facts. On the one hand, we and others have shown that SFV vectors mediate the induction of type I IFN responses triggered by RNA replication,[37] as well as the induction of apoptosis in tumor cells, which can lead to the release of tumor antigens that can be taken up by antigen-presenting cells to favor antitumor immune responses.[12] On the other hand, Gal3, as mentioned above, has numerous immunosuppressive functions and is considered an immune checkpoint.[46] One of these functions is the capacity to bind activated antigen-committed $CD8^+$ T cells, decreasing their function.[31–33,47] We demonstrated that Gal3-N-C12 displayed a potent effect in abrogating Gal3 binding to $CD8^+$ T cells stimulated with IL-10 and to $CD4^+$ T cells, with an efficacy similar to that of an anti-Gal3 antibody.[48] This inhibition was stronger in the $CD8^+PD1^+$ T cell population, which suggested that Gal3-N-C12 could improve the functionality of these activated cells. Interestingly, the N-terminal domain of Gal3 by itself (Gal3-N) was also able to inhibit Gal3 binding to $CD8^+$ and $CD4^+$ T cells. Gal3-N can interact with itself and with a part of the carbohydrate recognition domain (CRD) present in the C terminus of Gal3, forming a fuzzy complex via inter- and intramolecular interactions.[30,49] To our surprise, Gal3-C was not able to inhibit the binding of Gal3 to T cells, even though this molecule has been described as a dominant-negative form of Gal-3 and has been shown to reduce the growth of cultured ovarian cancer cells and control the progression of human breast

tumor xenografts in a nude mouse model.[29,50] It is possible that in our assay, Gal3-C, which contains the CRD, could interact with Gal3 to form hybrid complexes that could still efficiently bind to carbohydrates on the T cell surface. In fact, we did not observe antitumor effects in K7M2 osteosarcoma tumors treated with SFV-Gal3-C, confirming the lack of antitumor activity for this molecule.

In addition to inhibiting the binding of Gal3 to activated $CD8^+$ T cells, Gal3-N-C12 was able to significantly increase the infiltration of $CD8^+$ T cells in both primary tumors and pulmonary K7M2 metastases. A possibility that could explain this higher infiltration is that the Gal3-mediated sequestration of glycosylated cytokines, such as IL-12 and IFN-γ, could decrease the generation of chemokines required for T cell infiltration, such as CXCL9 and CXCL10.[23] An increase of DC was also observed in primary tumors, suggesting more cross-presentation of tumor antigens. In addition, our therapeutic treatment reduced the expression of IL-10, an immunosuppressive cytokine able to increase Gal3 binding to $CD8^+$ T cells, inhibiting their effector function.[46] Apart from increasing total $CD8^+$ T cell levels inside tumors, SFV-Gal3-N-C12 increased the number of tumor-specific $CD8^+$ T cells and decreased the $CD4^+$/$CD8^+$ T cell ratio, although this effect was also observed with the control SFV-Luc vector. This last parameter is considered a marker of a good prognosis and extended survival in osteosarcoma patients,[51] highlighting the therapeutic effect of our treatment strategy. An interesting observation was that $CD8^+$ T cells from tumors treated with SFV-Luc exhibited a more exhausted phenotype than those from tumors that received SFV-Gal3-N-C12, as indicated by the coexpression of the markers LAG3, PD1, and TIM3, which would help explain the difference in therapeutic efficacy between these two groups.

This therapeutic strategy also presented the advantage that viral replication will remain local, which reduces the potential risks and toxicities associated with using this virotherapy systemically.[52] Nevertheless, no life-threatening side effects attributed to Gal3 inhibitors were observed after systemic administration of the Gal3 inhibitor GR-MD-02 in the clinical trials NCT02117362 (GR-MD-02 and ipilimumab in patients with metastatic melanoma), NCT02575404 (GR-MD-02 and pembrolizumab in patients with metastatic melanoma, non-small cell lung cancer, or head and neck squamous cell carcinoma), and NCT00514696 (study of the safety of Gal3 antagonist GCS-100 in subjects with chronic lymphocytic leukemia). Moreover, the results from a first-in-human clinical trial evaluating the immunomodulatory effects and safety of Vvax001 (a replication-incompetent SFV vector-based cancer vaccine) in (pre-)malignant cervical lesions (NCT03141463) indicated that Vvax001 was safe and well tolerated and induced strong human papillomavirus (HPV) 16 E6- and E7-specific immune responses.[53]

In summary, our data underscore the potential therapeutic value of an SFV-Gal3-N-C12 vector as a therapeutic agent for patients affected by osteosarcoma, especially metastatic patients for whom no efficacious therapy is currently available.

MATERIALS AND METHODS

Cell lines and culture conditions

The hamster cell line BHK and the spontaneous murine osteosarcoma cell line K7M2 were obtained from American Type Culture Collection (Manassas, VA). The murine POS-1 and MOS-J cell lines, which were derived from spontaneous mouse osteosarcomas, were provided by Dr. Kamijo[54] and Dr. Shultz,[55] respectively, and were cultured in RPMI medium and DMEM, respectively, supplemented with 10% fetal bovine serum (FBS), 100 U/mL penicillin, and 100 μg/mL streptomycin. All cells were maintained in a humidified atmosphere with 5% CO_2 at 37°C. The cell lines were routinely tested for mycoplasma contamination (MycoAlert Mycoplasma Detection Kit; Lonza, Switzerland).

Viral vector construction

Three different mouse Gal3-derived constructs were designed and cloned into an SFV vector. Two of them were Gal3 inhibitors based on truncated forms of Gal3, Gal3-N-C12, and Gal3-C, which are based on the N-terminal domain of Gal3 (amino acids 1–135) linked to the Gal3 peptide inhibitor C-12[56] and on the Gal3 C-terminal domain (amino acids 122–264), respectively. In addition, two other constructs were generated to be used as controls, one containing Gal3-N and the other containing the peptide inhibitor C-12 (ANTPCGPYTHDCPVKR).[28] All constructs contained a signal peptide (SALLILALVGAAVA) at the amino-terminal end and an HA tag for detection, as indicated in Figure 2A. Synthetic DNA constructs encoding Gal3-N-C12, Gal3-C, and C-12 were supplied by GenScript (Nanjing, Hong Kong); they were all cloned into the pUC57 plasmid except for C-12, which was cloned into pcDNA3.1(−). All constructs were flanked by ApaI sites, which were used for subcloning each synthetic gene into pSFV-b1-2A,[57] generating pSFV-Gal3-N-C12, pSFV-Gal3-C, and pSFV-Gal3-C-12, respectively. pSFV-Gal3-N was obtained by digestion of pSFV-Gal3-N-C12 with NheI, whose restriction sites flanked the C-12 peptide sequence, and the purified plasmid was religated.

Generation of SFV viral particles

Synthetic RNAs were generated by *in vitro* transcription using SFV plasmids as templates and transfected into BHK-21 cells by electroporation. Both RNA synthesis and BHK-21 cell electroporation were performed as described previously.[58] To produce VPs to be used as therapeutic tools, SFV RNAs were packaged into VPs by coelectroporation of these RNAs together with two helper RNAs (SFV-helper-C-S219A and SFV-helper-S2), which provided the SFV capsid and envelope proteins, respectively, in *trans*.[59] Cells were incubated at 33°C for 48 h, and the supernatants were collected and used for the purification of SFV VPs by ultracentrifugation as described previously.[60] SFV-Luc was also produced.[57] The titers of each vector were determined by indirect immunofluorescence staining using a rabbit polyclonal antiserum specific for the nsp2 subunit of SFV replicase as the primary antibody[61] and an anti-rabbit immunoglobulin G (IgG) conjugated with Alexa Fluor 488 (Thermo Fisher, Waltham, MA) as the secondary antibody (Table S1).

Immunofluorescence staining

Indirect immunofluorescence staining was performed to detect the expression of recombinant proteins. BHK-21 cells were seeded in M6 wells and grown on coverslips for 24 h. The BHK-21 cells were then infected for 1 h with SFV VPs expressing Gal3 inhibitors. After 24 h, the infected cells were washed and fixed with methanol at −20°C for 20 min. Recombinant proteins were detected by using a primary anti-HA antibody (BioLegend, San Diego, CA) and a secondary anti-mouse IgG antibody conjugated with Alexa Fluor 488 (Thermo Fisher) (Table S1). Finally, the coverslips were placed on a microscope slide with a drop of Vectashield mounting medium containing DAPI (Vector Labs, Burlingame, CA) and visualized with a fluorescence microscope (Nikon, Japan).

In vitro infectivity

To assess the infectivity of SFV VPs *in vitro*, the K7M2 and MOS-J cell lines were plated on six-well plates at densities of 3×10^5 and 2×10^5, respectively, and infected with SFV-Gal3-N-C12 for 1 h at different MOIs. After 24 h the infected cells were fixed with methanol, and the SFV nsp2 replicase subunit was detected by indirect immunofluorescence staining.

RNA extraction and qRT-PCR

Gene expression analysis was assessed by qRT-PCR. RNA was extracted either from osteosarcoma cell lines using a Maxwell RNA extraction kit (Promega, Madison, WI) or from tibia and lung tissues using TRIzol reagent (Invitrogen, Waltham, MA) according to the manufacturer's protocols. RNA levels were quantified using a CFX96 real-time system (Bio-Rad, Hercules, CA) and an iQ SYBR-Green Supermix kit (Bio-Rad) with the following specific mouse primer sets: Gal-3: forward primer, 5′-CCA AAG AGG GAA TGA TGT TGC C-3′ and reverse primer, 5′-TGA TTG TAC TGC AAC AAG TGA GC-3′; Gal-3-BP: forward primer, 5′-CCA AAG AGG GAA TGA TGT TGC C-3′ and reverse primer, 5′-TGA TTG TAC TGC AAC AAG TGA GC-3′; IL-6: upstream primer, 5′-GTG TTG CCT GCT GCC TTC CCT G-3′ and downstream primer, 5′-CTC TAG GTA TAC CTC AAA CTC CAA-3′; C1GALT1: upstream primer, 5′-CAC CAC TTA ATC AAA GGT TAT CTA CCA A-3′ and downstream primer, 5′-AGG ACC CTC TAT GGG AGG ATA ATA G-3′; VLDLR: upstream primer, 5′-TGA CGC AGA CTG TTC AGA CC-3′ and downstream primer, 5′-GCC GTG GAT ACA GCT ACC AT-3′; ApoER2: upstream primer, 5′-AGA TGG GCT CAA CAG TCA CC-3′ and downstream primer, 5′-AGT GGG CGA TCA TAG TTG CT-3′; NC12: upstream primer, 5′-TCC ATC TGC TTA CCC AGG C-3′ and downstream primer, 5′-ACA GTC GTG TGT GTA AGG-3′; SFV rep: upstream primer, 5′-CTG TTC TCG ACG CGT CGT C-3′ and downstream primer, 5′-GAG GTG TTT CCA CGA CCC-3′. The following primers were used for human osteosarcoma cell lines: Gal-3: forward primer, 5′-CCA AAG AGG GAA TGA TGT TGC C-3′ and reverse primer, 5′-TGA TTG TAC TGC AAC AAG TGA GC-3′; Gal-3-BP: forward primer, 5′-GTG AAC GAT GGT GAC ATG CG-3′ and reverse primer, 5′-ATG ATG GGG CCT GAT CCT TG-3′.

Cell viability assay

The K7M2 and MOS-J cell lines were seeded at a density of 4×10^3 cells per well in 96-well plates and infected with SFV-Gal3-N, SFV-Gal3-C, SFV-Gal3-N-C12, SFV-C12, or SFV-Luc at MOIs ranging from 0 (mock) to 40. Cell viability was assessed 24 and 72 h after infection using a CellTiter-Glo Luminescent Cell Viability kit (Promega). The absorbance was measured using an Orion L Microplate Luminometer (Berthold Detection Systems, Pforzheim, Germany). The dose-response curves and IC_{50} values were analyzed using GraphPad Prism software (GraphPad Software, San Diego, CA).

Immunoblotting

Conditioned medium (CM) and CEs were collected 24 h after infection of BHK-21 cells with the different SFV VPs. CEs were obtained by treating samples with lysis buffer (PBS 1× + 1% Triton X-100) together with cOmplete, Mini Protease Inhibitor Cocktail (Sigma-Aldrich, St. Louis, MO) for 30 min on ice and centrifuging them for 20 min at 4°C. CM proteins were concentrated using 10% trichloroacetic acid (Merck, Kenilworth, NJ). Samples were subjected to SDS-Tris-Gly gel electrophoresis under denaturing conditions and then transferred to nitrocellulose membranes, which were incubated with antibodies specific for the following molecules (Table S1): nsp2 subunit of SFV replicase, HA tag (BioLegend), Gal3 (R&D Systems, Minneapolis, MN), Gal3-BP (ProteinTech, Rosemont, IL), and α-tubulin (Cell Signaling Technologies, Danvers, MA).

Gene expression analysis in osteosarcoma patients

Differential gene expression analysis of several genes of interest was performed by using the available gene expression data from a prior study performed by our laboratory group.[62] This study included processed microarray data for primary tumor and paired normal osteoblast samples that were obtained from six high-grade osteosarcoma patients before induction chemotherapy, by needle biopsy, and during surgery.

Animal studies

To establish osteosarcoma animal models, 5×10^5 K7M2 or 1×10^6 MOS-J cells were injected into female BALB/c and C57BL/6 mice, respectively, through the tibial plateau into the primary spongiosa of the right tibia. PBS or SFV (1×10^8 VPs per mouse) was administered intratumorally on day 7 after tumor engraftment. Tumor development and mouse weight were monitored twice weekly from the beginning of the experiment until the day of sacrifice. Tumor volumes were determined by measuring tumor size along two perpendicular diameters with a caliper and calculating the tumor volume with the following formula: Volume = $D \times (d)^2 \times 0.5$, where D is the largest diameter and d is the smaller diameter. The time point for sacrifice was set as the time when the tibial tumor volume reached 400 mm^3 or when the mice lost more than 20% of their body weight. Tibias were harvested to examine primary bone tumors, lungs were harvested to examine metastases, and livers were harvested to evaluate safety. The indicated organs were fixed with 3.7%–4.0% formaldehyde (PanReac AppliChem, Germany).

In vivo *infectivity assay*

Mice bearing orthotopically injected K7M2 cells were treated with 1×10^8 SFV-Luc VPs intratumorally 7 days after tumor engraftment. The mice were anesthetized with ketamine and xylazine, and luciferin (Sigma-Aldrich) was administered to the mice by intraperitoneal injection. Five minutes later, luciferase activity was recorded. Luciferase activity was measured every 2 days for up to 16 days with a Photon Imager Optima (Biospacelab, France). The luciferase signal was analyzed with Imaris software (Bitplane, Belfast, UK) and is expressed as the mean ± SD in photons per second.

Immunohistochemical analysis

Paraffin-embedded sections of mouse tibias and lungs were stained with H&E to analyze the presence of tumor regions and identify metastases in the lungs. Thereafter, these samples were immunostained following conventional procedures with an anti-CD3 antibody (clone SP7; NeoMarkers, Fremont, CA) and Vectastain ABC kits (Vector Labs) used according to the manufacturer's instructions. Quantification of CD3-stained cells was performed using ImageJ software (NIH, Bethesda, MD).

In vivo *pulmonary metastasis evaluation*

Thorax tomography was performed on day 23 after K7M2 cell inoculation. Mice were anesthetized by intraperitoneal injection of ketamine and xylazine and maintained on 2% inhaled isoflurane until they were completely relaxed. Mouse lung inhalation was controlled by placing an intratracheal cannula in mice connected to a flexiVent rodent ventilator (SCIREQ, Montreal, Canada), which was set at a rate of 200 breaths/min and a tidal volume of 10 mL/kg 3D.

Three-dimensional lung tomographic images were acquired using an X-ray microCT system (Quantum-GX; PerkinElmer, Waltham, MA, USA) with the following parameters: X-ray source voltage of 90 kVp, current of 88 μA, high-speed scan protocol for a total acquisition time of 4 min, and gantry rotation of 360°. Breathing artifacts were denoised using respiratory gating in each acquisition. Three-dimensional tomographic images containing the whole lung included a total of 512 slices with an isotropic voxel size of 72 μm and a resolution of 512×512 pixels per slice. Analysis of the lung volume in each sample was carried out using Fiji/ImageJ, which is open-source Java-based image-processing software. In brief, lung images were segmented by applying a fixed threshold, and total lung volume was measured over the obtained mask (mm^3).

Flow-cytometric analysis

The immune cell populations in primary K7M2 tumors and corresponding lung metastases were evaluated on days 3 and 7 after treatment. These tissues were processed by mechanical digestion and chemical digestion using DNase I and collagenase D (Sigma-Aldrich). The disaggregated cells were then passed through a 70-μm cell strainer and subjected to 30% Percoll (Fisher Scientific, Waltham, MA) treatment to obtain the tumor-infiltrating lymphocytes (TILs). For the identification of immune cell populations and evaluation of their phenotypic statuses, infiltrating immune cells were surface stained with the following antibodies resuspended in PBS containing 0.5% FBS and 0.5% EDTA: anti-mouse CD3 (clone 17A2), anti-mouse CD4 (clone GK1.5), anti-mouse CD8a (clone 53-6.7), anti-mouse CD11b (clone M1/70), anti-mouse CD11c (clone N418), anti-mouse CD19 (clone 6D5), anti-mouse CD25 (clone PC61), anti-mouse CD45 (clone 30-F11), anti-mouse CD206 (clone C068C2), anti-mouse F4/80 (clone BM8), anti-mouse Gal-3 (clone M3/38), anti-mouse IA/IE (clone M5/114.15.2), anti-mouse LAG3 (clone C9B7W), anti-mouse Ly6C (clone HK1.4), anti-mouse Ly6G (clone 1A8), anti-mouse NKP46 (clone 29A1.4), anti-mouse PD-1 (29F.1A12), anti-mouse TCRb (H57-597), and anti-mouse TIM3 (clone B8.2C12). For intracellular staining, cells were treated with Invitrogen Fixation/Permeabilization concentrate and diluent (Sigma-Aldrich) and stained with anti-mouse Foxp3 (clone FJK-16s), anti-mouse Granzyme B (clone NGZB), and anti-mouse IL-10 (clone JES5-16E3) antibodies (Table S2). PromoFluor-840 staining (1:10,000) was used to remove dead cells from the analysis (PromoCell, Heidelberg, Germany). An H-2Ld-restricted MuLV gp70-APC tetramer (MBL International, Woburn, MA) was used to identify tumor-specific $CD8^+$ T cells, as K7M2 cells have been shown to express the gp70 protein.[63] All samples were acquired on a CytoFLEX flow cytometer (Beckman Coulter, Brea, CA) with FACSDiva software (BD Biosciences, Franklin Lakes, NJ). Data analyses were performed using FlowJo v.10 (FlowJo, Ashland, OR) and SPICE software.[64]

IFN-γ ELISA and ELISPOT

K7M2 cells were cultured with recombinant murine IFN-γ (Fisher Scientific) at 100 IU/mL. Forty-eight hours later, splenocytes were isolated from K7M2 tumor-bearing mice that received different treatments and cocultured with irradiated K7M2 cells at an effector/target cell ratio of 40:1 (ELISA) or 10:1 (ELISPOT) in a 96-well plate for 72 h (ELISA) or 24 h (ELISPOT). Wells containing only splenocytes or K7M2 cells were used as controls for IFN-γ expression. For ELISA, the supernatant of each well was collected and analyzed using a mouse IFN-γ ELISA kit (BD Biosciences) following the manufacturer's instructions. For ELISPOT, a mouse IFN-γ ELISPOT kit (BD Biosciences, Franklin Lakes, NJ) was used according to the manufacturer's instructions. Results were measured using an IMMUNOSPOT S6 Macro Analyzer (CTL, Shaker Heights, OH).

Inhibition of the binding of Gal3 to the surface of $CD4^+$ and $CD8^+$ T cells

Splenocytes from BALB/c mice were collected, and $CD4^+$ or $CD8^+$ T cells were negatively isolated using a $CD4^+$ or $CD8^+$ T cell Isolation Kit Mouse (Miltenyi Biotec, Bergisch Gladbach, Germany), respectively. $CD4^+$ T cells were activated by incubation in anti-CD3-coated (1 μg/mL) and anti-CD28-coated (1 μg/mL) wells for 48 h. The cells were then placed in other plates and incubated with recombinant mouse Gal3 with an N-terminal 9His-2(SGGG)-IEGR tag (BioLegend) with or without recombinant Gal3 inhibitors (Gal-N-C12, Gal3-N, and Gal3-C) produced in *E. coli* from pET30a vectors (custom synthesized and purified by GenScript) or an anti-Gal3 antibody (clone B2C10; BD Pharmingen, San Diego, CA). Forty-eight hours later, the cells were

collected and prepared for staining with mouse anti-mouse CD45 (clone 30-F11), anti-mouse CD3 (clone 17A2), anti-mouse CD4 (clone GK1.5), anti-mouse PD1 (clone 29F.1A12), anti-mouse CD25 (clone PC61), and anti-mouse Gal3 (clone M3/38). Similarly, $CD8^+$ T cells were activated with anti-CD3 and anti-CD28 antibodies and recombinant mouse IL-10 (150 ng/mL; BioLegend) for 48 h. The $CD8^+$ T cells were then collected and cultured for 6 more days in the presence of recombinant mouse IL-10 without the anti-CD3 and anti-CD28 antibodies. On day 8, the $CD8^+$ T cells were collected and treated with Gal3 with or without Gal3 inhibitors (Gal-N-C12, Gal3-N, and Gal3-C) or anti-Gal3 (clone B2C10) for 30 min at 4°C. Finally, the $CD8^+$ T cells were collected and prepared for staining with mouse anti-mouse CD45 (clone 30-F11), anti-mouse CD3 (clone 17A2), anti-mouse CD8 (clone 53–6.7), anti-mouse PD1 (clone 29F.1A12), and anti-mouse Gal3 (clone M3/38).

Library preparation and RNA-seq

Primary tumor tissues were collected from orthotopic K7M2 tumor-bearing mice in TRIzol reagent (Invitrogen) on day 14 after intratumoral treatment with PBS, SFV-Luc, or SFV-Gal3-N-C12, as described above (n = 5). RNA was isolated from the tumor samples using TRIzol reagent following the manufacturer's instructions (Invitrogen). Thereafter, the isolated RNA was further purified and isolated using an RNeasy Mini Kit following the manufacturer's instructions (Qiagen, Hilden, Germany). RNA quantity and quality were tested with a Qubit (1.0) Fluorometer (Life Technologies, Carlsbad, CA) and High Sensitivity RNA ScreenTape following the manufacturer's instructions (Agilent, Waldbronn, Germany). Samples with an RNA integrity number (RIN) > 7 (based on the 28S/18S ratio) were processed with the stranded full-length RNA-seq mRNA preparation protocol by using a TruSeq RNA Sample Prep Kit according to manufacturer's instructions (Illumina, San Diego, CA). In brief, total RNA samples were poly(A) enriched with poly(T) oligo-conjugated magnetic beads and then reverse transcribed into double-stranded cDNA using random primers. The double-stranded cDNA samples were fragmented, end-repaired, and polyadenylated before ligation of TruSeq adapters containing the index for multiplexing. The fragments containing TruSeq adapters on both ends were selectively enriched by PCR. After PCR amplification, the enriched cDNA libraries were sequenced using a NextSeq2000 (Illumina).

Analysis of RNA-seq data

RNA-seq data analysis was performed using the following workflow: (1) the quality of the samples was verified using FastQC software (https://www.bioinformatics.babraham.ac.uk/projects/fastqc/), (2) the alignment of reads to a mouse genome (mm10) was performed using STAR,[65] (3) gene expression quantification using read counts of exonic gene regions was carried out with featureCounts,[66] (4) the gene annotation reference was Gencode M25,[67] and (5) differential expression statistical analysis was performed using R/Bioconductor.[68] Data are publicly available from the Gene Expression Omnibus database under the accession number GEO: GSE197902.

First, gene expression data were normalized with edgeR[69] and voom.[70] After quality assessment and outlier detection using R/Bioconductor,[68] a filtering process was performed. Genes with read counts lower than 6 in more than 50% of the samples for all the studied conditions were considered not expressed in the experiment under study. LIMMA[70] was used to identify the genes with significant differential expression between the experimental conditions. Genes were selected as differentially expressed using a cutoff of $p < 0.01$. Further functional and clustering analyses were performed, and graphical representations were generated using clusterProfiler[71] and R/Bioconductor.[68]

The functional analyses included gene set enrichment analysis (GSEA) with the MsigDB C7 collection of gene sets.[71,72] This collection contains gene sets that represent cell states and perturbations within the immune system. In addition, GSEA was performed using a gene set of prometastatic genes previously described to favor metastasis in osteosarcomas.[34] For this analysis, $p < 0.01$ and false discovery rate of $q < 0.05$ were considered statistically significant.

To evaluate changes in the tumor microenvironment, we analyzed the abundances of immune cell populations in primary tumors after treating K7M2 tumor-bearing mice with PBS, SFV-Luc, or SFV-Gal3-N-C12 using the online tool ImmuCellAI-mouse.[73] We further analyzed the expression of interesting immunomodulatory molecules in primary tumors among the treatment groups. The expression of the selected immunomodulatory genes is represented in a heatmap.

Statistical analysis

Data from *in vitro* and *ex vivo* studies are expressed as the mean ± SD. Statistical comparisons were performed by applying a convenient two-tailed Student's t test or ANOVA followed by Tukey's multiple comparison test, as indicated in each figure legend. For *in vivo* studies, survival differences among treated groups are represented by Kaplan-Meier plots, and survival curves were compared using the log-rank test. For time-series analysis (tumor growth curves), data were compared using the extra sum-of-squares F test in the Prism software package and fitted to a second-order polynomial equation. GraphPad Prism 9 software was used for all statistical analyses. p values of <0.05 were considered statistically significant.

Study approval

The Ethical Committee of the University of Navarra (Comite Etico de Experimentacion Animal (CEEA)) approved the animal protocols performed in this study (CEEA/044-21).

All animal studies were performed at the animal facilities of Cima Universidad de Navarra following institutional, regional, and national laws and ethical guidelines for experimental animal care.

Data and materials availability

The data that support the findings of this study are available within the paper or supplemental information or are available from the corresponding author upon request.

SUPPLEMENTAL INFORMATION

Supplemental information can be found online at https://doi.org/10.1016/j.omto.2022.07.004.

ACKNOWLEDGMENTS

We would like to thank personnel at the Cima Universidad de Navarra animal, genomic, and bioinformatics facilities for excellent help. Funding: the performed work was supported through the Departamento de Salud del Gobierno de Navarra (54/2018-APG); Predoctoral Fellowship from Gobierno de Navarra (G.H.-C. and V.L.), Instituto de Salud Carlos III y Fondos Feder (PI19/01896 [M.M.A.], PI18/00164 [A.P.-G.], PI17/01859 and PI20/00415 [C.S.]; "A Way to Make Europe"); Amigos de la Universidad de Navarra (to M.P.); "Ayudas predoctorales de investigación biomédica AC" (to N.S.-P.); Fundación La Caixa/Caja Navarra (A.P.-G. and M.M.A.); Fundación El sueño de Vicky; Asociación Pablo Ugarte-FuerzaJulen, Fundación ADEY, Fundación ACS (A.P.-G. and M.M.A.); La Marató (M.M.A.). Gobierno de Navarra Industria (0011-1411-2019-000079; Proyecto DESCARTHeS to C.S.), and Gobierno de Navarra. Departamento de Salud 64/2019 (to C.S., cofinanced at 50% by the European Regional Development Fund through the FEDER Operational Program 2014–2020 of Navarra: "European Union. European Regional Development Fund. A Way to Make Europe"). This project also received funding from the European Research Council (ERC) under the European Union's Horizon 2020 Research and Innovation Program (817884 ViroPedTher to M.M.A.).

AUTHOR CONTRIBUTIONS

Conception and design, G.H.-C., R.H.-A., C.S., and M.M.A.; development of methodology, all authors; acquisition of data (provided animals, acquired and managed patients, provided facilities), all authors; analysis and interpretation of the data (statistical analysis, biostatistics, computational analysis), all authors; writing, review, and/or revision of the manuscript, all authors; administrative, technical, or material support (reporting or organizing data and constructing databases), all authors; study supervision, S.L., R.H.-A., C.S., and M.M.A.

DECLARATION OF INTERESTS

M.M.A. has a research grant from DNAtrix not related to this study.

REFERENCES

1. Ottaviani, G., and Jaffe, N. (2009). The epidemiology of osteosarcoma. Cancer Treat. Res. *152*, 3–13.
2. Abarrategi, A., Tornin, J., Martinez-Cruzado, L., Hamilton, A., Martinez-Campos, E., Rodrigo, J.P., González, M.V., Baldini, N., Garcia-Castro, J., and Rodriguez, R. (2016). Osteosarcoma: cells-of-origin, cancer stem cells, and targeted therapies. Stem Cell. Int. *2016*, 3631764.
3. Muhsin Chisti, M. (2019). Osteogenic Sarcoma Treatment Protocols (Medscape).
4. Mirabello, L., Troisi, R.J., and Savage, S.A. (2009). Osteosarcoma incidence and survival rates from 1973 to 2004: data from the surveillance, epidemiology, and end results program. Cancer *115*, 1531–1543.
5. Chaurasiya, S., Fong, Y., and Warner, S.G. (2021). Oncolytic virotherapy for cancer: clinical experience. Biomedicines *9*, 419.
6. Heikkilä, J.E., Vähä-Koskela, M.J.V., Ruotsalainen, J.J., Martikainen, M.W., Stanford, M.M., McCart, J.A., Bell, J.C., and Hinkkanen, A.E. (2010). Intravenously administered alphavirus vector VA7 eradicates orthotopic human glioma xenografts in nude mice. PLoS One *5*, e8603.
7. Quetglas, J.I., Fioravanti, J., Ardaiz, N., Medina-Echeverz, J., Baraibar, I., Prieto, J., Smerdou, C., and Berraondo, P. (2012). A Semliki forest virus vector engineered to express IFNalpha induces efficient elimination of established tumors. Gene Ther. *19*, 271–278.
8. Quetglas, J.I., Labiano, S., Aznar, M.Á., Bolaños, E., Azpilikueta, A., Rodriguez, I., Casales, E., Sánchez-Paulete, A.R., Segura, V., Smerdou, C., and Melero, I. (2015). Virotherapy with a Semliki forest virus-based vector encoding IL12 synergizes with PD-1/PD-L1 blockade. Cancer Immunol. Res. *3*, 449–454.
9. Martikainen, M., Ramachandran, M., Lugano, R., Ma, J., Martikainen, M.M., Dimberg, A., Yu, D., Merits, A., and Essand, M. (2021). IFN-I-tolerant oncolytic Semliki Forest virus in combination with anti-PD1 enhances T cell response against mouse glioma. Mol. Ther. Oncolytics *21*, 37–46.
10. Autio, K.P.M., Ruotsalainen, J.J., Anttila, M.O., Niittykoski, M., Waris, M., Hemminki, A., Vähä-Koskela, M.J.V., and Hinkkanen, A.E. (2015). Attenuated Semliki Forest virus for cancer treatment in dogs: safety assessment in two laboratory Beagles. BMC Vet. Res. *11*, 170.
11. Ketola, A., Hinkkanen, A., Yongabi, F., Furu, P., Määttä, A.M., Liimatainen, T., Pirinen, R., Björn, M., Hakkarainen, T., Mäkinen, K., et al. (2008). Oncolytic Semliki forest virus vector as a novel candidate against unresectable osteosarcoma. Cancer Res. *68*, 8342–8350.
12. Quetglas, J.I., Ruiz-Guillen, M., Aranda, A., Casales, E., Bezunartea, J., and Smerdou, C. (2010). Alphavirus vectors for cancer therapy. Virus Res. *153*, 179–196.
13. Lei, P., He, H., Hu, Y., and Liao, Z. (2015). Small interfering RNA-induced silencing of galectin-3 inhibits the malignant phenotypes of osteosarcoma in vitro. Mol. Med. Rep. *12*, 6316–6322.
14. Zhou, X., Jing, J., Peng, J., Mao, W., Zheng, Y., Wang, D., Wang, X., Liu, Z., and Zhang, X. (2014). Expression and clinical significance of galectin-3 in osteosarcoma. Gene *546*, 403–407.
15. Nakajima, K., Kho, D.H., Yanagawa, T., Zimel, M., Heath, E., Hogan, V., and Raz, A. (2016). Galectin-3 in bone tumor microenvironment: a beacon for individual skeletal metastasis management. Cancer Metastasis. Rev. *35*, 333–346.
16. Fortuna-Costa, A., Gomes, A.M., Kozlowski, E.O., Stelling, M.P., and Pavão, M.S.G. (2014). Extracellular galectin-3 in tumor progression and metastasis. Front. Oncol. *4*, 138.
17. Park, G.B., Kim, D.J., Kim, Y.S., Lee, H.K., Kim, C.W., and Hur, D.Y. (2015). Silencing of galectin-3 represses osteosarcoma cell migration and invasion through inhibition of FAK/Src/Lyn activation and beta-catenin expression and increases susceptibility to chemotherapeutic agents. Int. J. Oncol. *46*, 185–194.
18. Fukumori, T., Kanayama, H.O., and Raz, A. (2007). The role of galectin-3 in cancer drug resistance. Drug Resist. Updat. *10*, 101–108.
19. Harazono, Y., Kho, D.H., Balan, V., Nakajima, K., Hogan, V., and Raz, A. (2015). Extracellular galectin-3 programs multidrug resistance through Na+/K+-ATPase and P-glycoprotein signaling. Oncotarget *6*, 19592–19604.
20. Nakajima, K., Balan, V., and Raz, A. (2021). Galectin-3: an immune checkpoint target for musculoskeletal tumor patients. Cancer Metastasis. Rev. *40*, 297–302.
21. Jia, W., Kidoya, H., Yamakawa, D., Naito, H., and Takakura, N. (2013). Galectin-3 accelerates M2 macrophage infiltration and angiogenesis in tumors. Am. J. Pathol. *182*, 1821–1831.
22. Silverman, A.M., Nakata, R., Shimada, H., Sposto, R., and DeClerck, Y.A. (2012). A galectin-3-dependent pathway upregulates interleukin-6 in the microenvironment of human neuroblastoma. Cancer Res. *72*, 2228–2238.
23. Gordon-Alonso, M., Hirsch, T., Wildmann, C., and van der Bruggen, P. (2017). Galectin-3 captures interferon-gamma in the tumor matrix reducing chemokine gradient production and T-cell tumor infiltration. Nat. Commun. *8*, 793.
24. Kouo, T., Huang, L., Pucsek, A.B., Cao, M., Solt, S., Armstrong, T., and Jaffee, E. (2015). Galectin-3 shapes antitumor immune responses by suppressing CD8+ T cells via LAG-3 and inhibiting expansion of plasmacytoid dendritic cells. Cancer Immunol. Res. *3*, 412–423.

25. Chen, H.Y., Fermin, A., Vardhana, S., Weng, I.C., Lo, K.F.R., Chang, E.Y., Maverakis, E., Yang, R.Y., Hsu, D.K., Dustin, M.L., and Liu, F.T. (2009). Galectin-3 negatively regulates TCR-mediated CD4+ T-cell activation at the immunological synapse. Proc. Natl. Acad. Sci. USA *106*, 14496–14501.

26. Peng, W., Wang, H.Y., Miyahara, Y., Peng, G., and Wang, R.F. (2008). Tumor-associated galectin-3 modulates the function of tumor-reactive T cells. Cancer Res. *68*, 7228–7236.

27. Gross, A.C., Cam, H., Phelps, D.A., Saraf, A.J., Bid, H.K., Cam, M., London, C.A., Winget, S.A., Arnold, M.A., Brandolini, L., et al. (2018). IL-6 and CXCL8 mediate osteosarcoma-lung interactions critical to metastasis. JCI Insight *3*, 99791.

28. Zou, J., Glinsky, V.V., Landon, L.A., Matthews, L., and Deutscher, S.L. (2005). Peptides specific to the galectin-3 carbohydrate recognition domain inhibit metastasis-associated cancer cell adhesion. Carcinogenesis *26*, 309–318.

29. John, C.M., Leffler, H., Kahl-Knutsson, B., Svensson, I., and Jarvis, G.A. (2003). Truncated galectin-3 inhibits tumor growth and metastasis in orthotopic nude mouse model of human breast cancer. Clin. Cancer Res. *9*, 2374–2383.

30. Chiu, Y.P., Sun, Y.C., Qiu, D.C., Lin, Y.H., Chen, Y.Q., Kuo, J.C., and Huang, J.R. (2020). Liquid-liquid phase separation and extracellular multivalent interactions in the tale of galectin-3. Nat. Commun. *11*, 1229.

31. Demotte, N., Wieërs, G., Van Der Smissen, P., Moser, M., Schmidt, C., Thielemans, K., Squifflet, J.L., Weynand, B., Carrasco, J., Lurquin, C., et al. (2010). A galectin-3 ligand corrects the impaired function of human CD4 and CD8 tumor-infiltrating lymphocytes and favors tumor rejection in mice. Cancer Res. *70*, 7476–7488.

32. Sasawatari, S., Okamoto, Y., Kumanogoh, A., and Toyofuku, T. (2020). Blockade of N-glycosylation promotes antitumor immune response of T cells. J. Immunol. *204*, 1373–1385.

33. Petit, A.E., Demotte, N., Scheid, B., Wildmann, C., Bigirimana, R., Gordon-Alonso, M., Carrasco, J., Valitutti, S., Godelaine, D., and van der Bruggen, P. (2016). A major secretory defect of tumour-infiltrating T lymphocytes due to galectin impairing LFA-1-mediated synapse completion. Nat. Commun. *7*, 12242.

34. Maximov, V.V., and Aqeilan, R.I. (2016). Genetic factors conferring metastasis in osteosarcoma. Future Oncol. *12*, 1623–1644.

35. Farhad, M., Rolig, A.S., and Redmond, W.L. (2018). The role of Galectin-3 in modulating tumor growth and immunosuppression within the tumor microenvironment. Oncoimmunology *7*, e1434467.

36. Ruvolo, P.P. (2016). Galectin 3 as a guardian of the tumor microenvironment. Biochim. Biophys. Acta *1863*, 427–437.

37. Melero, I., Quetglas, J.I., Reboredo, M., Dubrot, J., Rodriguez-Madoz, J.R., Mancheño, U., Casales, E., Riezu-Boj, J.I., Ruiz-Guillen, M., Ochoa, M.C., et al. (2015). Strict requirement for vector-induced type I interferon in efficacious antitumor responses to virally encoded IL12. Cancer Res. *75*, 497–507.

38. Jiang, W., He, Y., He, W., Wu, G., Zhou, X., Sheng, Q., Zhong, W., Lu, Y., Ding, Y., Lu, Q., et al. (2020). Exhausted CD8+T cells in the tumor immune microenvironment: new pathways to therapy. Front. Immunol. *11*, 622509.

39. Zheng, W., Xiao, H., Liu, H., and Zhou, Y. (2015). Expression of programmed death 1 is correlated with progression of osteosarcoma. APMIS *123*, 102–107.

40. Kozawa, E., Sugiura, H., Wasa, J., Kohyama, K., Yamada, K., Nishioka, A., Nishida, Y., Ishiguro, N., and Taguchi, O. (2010). Suppression of tumour metastasis in a murine osteosarcoma model with anti-CD25 monoclonal antibody treatment. Anticancer Res. *30*, 5019–5022.

41. Cao, F., Nguyen, P., Hong, B., DeRenzo, C., Rainusso, N.C., Rodriguez Cruz, T., Wu, M.F., Liu, H., Song, X.T., Suzuki, M., et al. (2021). Engineering oncolytic vaccinia virus to redirect macrophages to tumor cells. Adv. Cell Gene Ther. *4*, e99.

42. Martinez-Velez, N., Laspidea, V., Zalacain, M., Labiano, S., Garcia-Moure, M., Puigdelloses, M., Marrodan, L., Gonzalez-Huarriz, M., Herrador, G., de la Nava, D., et al. (2021). Local treatment of a pediatric osteosarcoma model with a 4-1BBL armed oncolytic adenovirus results in an antitumor effect and leads to immune memory. Mol. Cancer Ther. *21*, 471–480.

43. Cortini, M., Massa, A., Avnet, S., Bonuccelli, G., and Baldini, N. (2016). Tumor-activated mesenchymal stromal cells promote osteosarcoma stemness and migratory potential via IL-6 secretion. PLoS One *11*, e0166500.

44. Han, X.G., Mo, H.M., Liu, X.Q., Li, Y., Du, L., Qiao, H., Fan, Q.M., Zhao, J., Zhang, S.H., and Tang, T.T. (2018). TIMP3 overexpression improves the sensitivity of osteosarcoma to cisplatin by reducing IL-6 production. Front. Genet. *9*, 135.

45. Itoh, H., Kadomatsu, T., Tanoue, H., Yugami, M., Miyata, K., Endo, M., Morinaga, J., Kobayashi, E., Miyamoto, T., Kurahashi, R., et al. (2018). TET2-dependent IL-6 induction mediated by the tumor microenvironment promotes tumor metastasis in osteosarcoma. Oncogene *37*, 2903–2920.

46. Compagno, D., Tiraboschi, C., Garcia, J.D., Rondón, Y., Corapi, E., Velazquez, C., and Laderach, D.J. (2020). Galectins as checkpoints of the immune system in cancers, their clinical relevance, and implication in clinical trials. Biomolecules *10*, E750.

47. Demotte, N., Stroobant, V., Courtoy, P.J., Van Der Smissen, P., Colau, D., Luescher, I.F., Hivroz, C., Nicaise, J., Squifflet, J.L., Mourad, M., et al. (2008). Restoring the association of the T cell receptor with CD8 reverses anergy in human tumor-infiltrating lymphocytes. Immunity *28*, 414–424.

48. Smith, L.K., Boukhaled, G.M., Condotta, S.A., Mazouz, S., Guthmiller, J.J., Vijay, R., Butler, N.S., Bruneau, J., Shoukry, N.H., Krawczyk, C.M., and Richer, M.J. (2018). Interleukin-10 directly inhibits CD8(+) T cell function by enhancing N-glycan branching to decrease antigen sensitivity. Immunity *48*, 299–312.e5.

49. Lin, Y.H., Qiu, D.C., Chang, W.H., Yeh, Y.Q., Jeng, U.S., Liu, F.T., and Huang, J.R. (2017). The intrinsically disordered N-terminal domain of galectin-3 dynamically mediates multisite self-association of the protein through fuzzy interactions. J. Biol. Chem. *292*, 17845–17856.

50. Mirandola, L., Yu, Y., Cannon, M.J., Jenkins, M.R., Rahman, R.L., Nguyen, D.D., Grizzi, F., Cobos, E., Figueroa, J.A., and Chiriva-Internati, M. (2014). Galectin-3 inhibition suppresses drug resistance, motility, invasion and angiogenic potential in ovarian cancer. Gynecol. Oncol. *135*, 573–579.

51. Morales-Molina, A., Gambera, S., Leo, A., and García-Castro, J. (2021). Combination immunotherapy using G-CSF and oncolytic virotherapy reduces tumor growth in osteosarcoma. J. Immunother. Cancer *9*, e001703.

52. Dumic, J., Dabelic, S., and Flögel, M. (2006). Galectin-3: an open-ended story. Biochim. Biophys. Acta *1760*, 616–635.

53. Komdeur, F.L., Singh, A., van de Wall, S., Meulenberg, J.J.M., Boerma, A., Hoogeboom, B.N., Paijens, S.T., Oyarce, C., de Bruyn, M., Schuuring, E., et al. (2021). First-in-Human phase I clinical trial of an SFV-based RNA replicon cancer vaccine against HPV-induced cancers. Mol. Ther. *29*, 611–625.

54. Kamijo, A., Koshino, T., Uesugi, M., Nitto, H., and Saito, T. (2002). Inhibition of lung metastasis of osteosarcoma cell line POS-1 transplanted into mice by thigh ligation. Cancer Lett. *188*, 213–219.

55. Joliat, M.J., Umeda, S., Lyons, B.L., Lynes, M.A., and Shultz, L.D. (2002). Establishment and characterization of a new osteogenic cell line (MOS-J) from a spontaneous C57BL/6J mouse osteosarcoma. In Vivo *16*, 223–228.

56. Sun, W., Li, L., Yang, Q., Shan, W., Zhang, Z., and Huang, Y. (2015). G3-C12 peptide reverses galectin-3 from foe to friend for active targeting cancer treatment. Mol. Pharmacol. *12*, 4124–4136.

57. Rodriguez-Madoz, J.R., Prieto, J., and Smerdou, C. (2005). Semliki forest virus vectors engineered to express higher IL-12 levels induce efficient elimination of murine colon adenocarcinomas. Mol. Ther. *12*, 153–163.

58. Liljeström, P., and Garoff, H. (1994). Expression of proteins using Semliki forest virus vectors: protein expression. Curr. Protoc. Mol. Biol. *25*, 16.20.1–16.20.16.

59. Smerdou, C., and Liljeström, P. (1999). Two-helper RNA system for production of recombinant Semliki forest virus particles. J. Virol. *73*, 1092–1098.

60. Fleeton, M.N., Sheahan, B.J., Gould, E.A., Atkins, G.J., and Liljestr M, P. (1999). Recombinant Semliki Forest virus particles encoding the prME or NS1 proteins of louping ill virus protect mice from lethal challenge. J. Gen. Virol. *80*, 1189–1198.

61. Casales, E., Rodriguez-Madoz, J.R., Ruiz-Guillen, M., Razquin, N., Cuevas, Y., Prieto, J., and Smerdou, C. (2008). Development of a new noncytopathic Semliki Forest virus vector providing high expression levels and stability. Virology *376*, 242–251.

62. Patiño-García, A., Zalacain, M., Folio, C., Zandueta, C., Sierrasesúmaga, L., San Julián, M., Toledo, G., De Las Rivas, J., and Lecanda, F. (2009). Profiling of chemonaive osteosarcoma and paired-normal cells identifies EBF2 as a mediator of osteoprotegerin inhibition to tumor necrosis factor-related apoptosis-inducing ligand-induced apoptosis. Clin. Cancer Res. *15*, 5082–5091.

63. Wedekind, M.F., Miller, K.E., Chen, C.Y., Wang, P.Y., Hutzen, B.J., Currier, M.A., Nartker, B., Roberts, R.D., Boon, L., Conner, J., et al. (2021). Endogenous retrovirus envelope as a tumor-associated immunotherapeutic target in murine osteosarcoma. iScience *24*, 102759.

64. Roederer, M., Nozzi, J.L., and Nason, M.C. (2011). SPICE: exploration and analysis of post-cytometric complex multivariate datasets. Cytometry. A *79*, 167–174.

65. Dobin, A., Davis, C.A., Schlesinger, F., Drenkow, J., Zaleski, C., Jha, S., Batut, P., Chaisson, M., and Gingeras, T.R. (2013). STAR: ultrafast universal RNA-seq aligner. Bioinformatics *29*, 15–21.

66. Liao, Y., Smyth, G.K., and Shi, W. (2014). featureCounts: an efficient general purpose program for assigning sequence reads to genomic features. Bioinformatics *30*, 923–930.

67. Harrow, J., Frankish, A., Gonzalez, J.M., Tapanari, E., Diekhans, M., Kokocinski, F., Aken, B.L., Barrell, D., Zadissa, A., Searle, S., et al. (2012). GENCODE: the reference human genome annotation for the ENCODE Project. Genome Res. *22*, 1760–1774.

68. Gentleman, R.C., Carey, V.J., Bates, D.M., Bolstad, B., Dettling, M., Dudoit, S., Ellis, B., Gautier, L., Ge, Y., Gentry, J., et al. (2004). Bioconductor: open software development for computational biology and bioinformatics. Genome Biol. *5*, R80.

69. Robinson, M.D., McCarthy, D.J., and Smyth, G.K. (2010). edgeR: a Bioconductor package for differential expression analysis of digital gene expression data. Bioinformatics *26*, 139–140.

70. Ritchie, M.E., Phipson, B., Wu, D., Hu, Y., Law, C.W., Shi, W., and Smyth, G.K. (2015). Limma powers differential expression analyses for RNA-sequencing and microarray studies. Nucleic Acids Res. *43*, e47.

71. Yu, G., Wang, L.G., Han, Y., and He, Q.Y. (2012). clusterProfiler: an R package for comparing biological themes among gene clusters. OMICS *16*, 284–287.

72. Subramanian, A., Tamayo, P., Mootha, V.K., Mukherjee, S., Ebert, B.L., Gillette, M.A., Paulovich, A., Pomeroy, S.L., Golub, T.R., Lander, E.S., and Mesirov, J.P. (2005). Gene set enrichment analysis: a knowledge-based approach for interpreting genome-wide expression profiles. Proc. Natl. Acad. Sci. USA *102*, 15545–15550.

73. Miao, Y.R., Xia, M., Luo, M., Luo, T., Yang, M., and Guo, A.Y. (2021). ImmuCellAI-mouse: a tool for comprehensive prediction of mouse immune cell abundance and immune microenvironment depiction. Bioinformatics *38*, 785–791.